We are IntechOpen, the world's leading publisher of Open Access books Built by scientists, for scientists

6,900
Open access books available

186,000
International authors and editors

200M
Downloads

Our authors are among the

154
Countries delivered to

TOP 1%
most cited scientists

12.2%
Contributors from top 500 universities

WEB OF SCIENCE™

Selection of our books indexed in the Book Citation Index in Web of Science™ Core Collection (BKCI)

Interested in publishing with us?
Contact book.department@intechopen.com

Numbers displayed above are based on latest data collected.
For more information visit www.intechopen.com

Chapter 9

Some Unitary, Binary, and Ternary Non-TiO_2 Photocatalysts

Martyna Marchelek, Magdalena Diak, Magda Kozak, Adriana Zaleska-Medynska and Ewelina Grabowska

Additional information is available at the end of the chapter

http://dx.doi.org/10.5772/62583

Abstract

Among all kinds of green earth and renewable energy projects underway, semiconductor photocatalysis has received wide interest because it provides an easy way to directly utilize the energy of either natural sunlight or artificial indoor illumination. TiO_2, the most widely used photocatalyst, due to its wide band gap, can only be activated under UV irradiation, and thus, the development of novel semiconductor photocatalysts makes a significant advancement in photocatalytic functional materials. One of the effective strategies to overcome this shortcoming is photosensitizing these wide band gap semiconductors with narrow band gap semiconductors which have proper energy levels. This method can not only improve the photocatalytic activity, due to increasing visible-light-harvesting efficiency, but also can decrease the recombination of the charge carriers, because the formation of *n*–*n* or *n*–*p* heterojunctions between the combined semiconductors can induce internal electric fields between them. In this regard, this review presents some unitary, binary, and ternary non-TiO_2 photocatalysts used for the degradation for organic pollutants and for water splitting.

Keywords: semiconductor photocatalysis, non-TiO_2 photocatalysts, composite photocatalysts, pollutant degradation, photoactivity under UV–Vis or visible light

1. Introduction

Among the various Advanced Oxidation Process methods, semiconductor-mediated photocatalysis has been accorded a great significance in recent times due to its potential to mineralize

INTECH
open science | open minds

© 2016 The Author(s). Licensee InTech. This chapter is distributed under the terms of the Creative Commons Attribution License (http://creativecommons.org/licenses/by/3.0), which permits unrestricted use, distribution, and reproduction in any medium, provided the original work is properly cited. CC BY

a wide range of organic pollutants at ambient temperature and pressures into harmless substances, to produce hydrogen in photocatalytic water-splitting process, and to apply in dye-sensitized solar cells [1–3].

From the simple oxides (e.g., TiO_2, ZnO, WO_3, Fe_2O_3), anatase–TiO_2 is a dominant structure employed for sunlight applications mostly due to its charge carrier handling properties. However, the TiO_2-based photocatalyst cannot effectively absorb visible solar light due to a rather large band gap (>3.2 eV), rendering it of little practical significance for solar energy harvesting. Additionally, pure TiO_2 used during photocatalytic processes has few disadvantages, such as low quantum yield due to a high recombination rate between photogenerated electron–hole pairs, or the need of high-energy photons to activate the semiconductors in the UV region.

Qu et al. [4] pointed that designing of an efficient and stable photocatalysts must follow several critical requirements: (*i*) Semiconductor must have band gap large enough to provide energetic electrons and smaller enough to allow for efficient absorption overlap with the solar spectrum (1.23 eV $\ll E_g \ll$ 3.0 eV, typically >2.0 eV); (*ii*) there must be a mechanism to efficiently drive charge separation and the transportation process; and (*iii*) there must be a mechanism to efficiently drive charge separation and the transportation process.

Because, in most cases, single semiconductors are unlikely to satisfy all these requirements, one of the important issues in the photocatalysis fields is to exploit new combining of some semiconductors to form composites which can improve the efficiency of a photocatalytic system. This fact provides an excellent opportunity to continue developing new materials with higher photocatalytic activity and capable to use the sunlight as a green energy source.

The current review is focused on non-TiO_2 materials with particular emphasis placed on application of these photocatalysts in heterogeneous photocatalysis and insight into explanation the photocatalytic mechanism of the composite photocatalyst. This review is organized into four sections: (1) single-semiconductor photocatalysts for pollutant degradation, (2) single-semiconductor photocatalysts for water splitting, (3) semiconductor composite photocatalysts, and (4) conclusions and perspectives.

2. Single-semiconductor photocatalysts for pollutant degradation

In general, fundamental principles of photodegradation mechanism was based on oxidation and reduction reactions of induced charged carriers. Ultimately, in both reactions from water oxidation and dissociation of H_2O_2, hydroxyl radical could be produced, which are highly powerful and nonselective oxidizing agent. During the past few years, numerous efforts have been made for the discovery of new visible-light-responding semiconductors. Among the created groups of photocatalysts, the biggest part in the literature belongs to ferrates, halides, oxides, tungstates, sulfides, and vanadates. All the groups utilized recently in heterogeneous photocatalysis are listed in **Table 1**, while band gap values for selected groups of photocatalyst are shown in **Figure 1**.

http://dx.doi.org/10.5772/62583

Recently, metal sulfides received much attention because their promising properties. CdS is one of the intensively investigated semiconductors owing to the narrow band gap (2.1–2.5 eV) in comparison with TiO_2 which may extend the utilization of visible light. For instance, Eskandari et al. [99] synthesized CdS by simple chemical precipitation method using mercaptoethylamine hydrochloride (MEA) as a capping agent. CdS showed higher photocatalytic activity than P25-TiO_2 in the photodegradation of methylene blue under blue LED and solar light irradiation. Reusability of the photocatalyst was checked five times; during the first three times, the activity decreased gradually, but in the last two cycles, they observed very sharp drop in photoactivity. Chen et al. [100] also observed higher activity of CdS in comparison with P25-TiO_2, after 60 min of UV irradiation nearly 95% of rhodamine B (RhB) was degraded. The band gap (2.24 eV) was calculated according to the UV–Vis absorption spectra [100]. Another very often mentioned material is ZnS. Chen et al. used ZnS rods as photocatalysts for the degradation of methyl orange (95% of MO was degraded after 20 min) and 2,4-dinitrophenol (54% of 2,4-NP was degraded after 20 min) under UV irradiation [105]. ZnS with a band gap equals to 3.84 eV exceeded activity of commercial P25-TiO_2. Chen et al. also proposed photocatalytic degradation mechanism of OM and 2,4-NP over ZnS under UV light. For this reason, EDTA-Na_2 and potassium iodide (KI) were introduced as the scavengers for h^+, isopropanol, and ethanol were used for $^{\bullet}OH$, and 1,4-benzoquinone for $^{\bullet}O_2^-$, respectively. They confirmed that the photocatalytic process proceeds analogously like for TiO_2, and thus, h^+ and $^{\bullet}O_2^-$ are the crucial in the degradation pathway under UV irradiation [105]. Chen et al. [115] applied simple wet chemical method for obtaining Bi_2S_3. The photocatalytic activity was measured by methyl orange degradation in the presence of UV light. After 4 h of irradiation, 97% of methyl orange was decolorized in the presence of Bi_2S_3 photocatalyst with specific surface area about 20 $m^2\ g^{-1}$ [115]. Luo et al. [116] performed Bi_2S_3 nanorods which exhibited superior activity than P25-TiO_2 in rhodamine B degradation under visible light ($\lambda > 420$ nm).

Another extensively examined groups are wide band gap oxides such as ZnO, WO_3, Nb_2O_5, and Bi_2O_3. Nanosized ZnO photocatalysts were synthesized by Liu et al. Obtained samples exhibited high activity in methyl orange degradation under UV light. After 30 min irradiation, the efficiency was nearly 100%. ZnO was proved to be very stable during 4 cycles. In many publications, some of the photocatalysts are perceived as a narrow band gap semiconductor such as Bi_2O_3, CeO_2, Fe_2O_3, and WO_3. This dispersion in the values of the band gap is inter alia due to different preparation method. Zheng et al. [166] synthesized WO_3 nanorod arrays by hydrothermal method, and the results showed that the pH value of the precursor solutions plays crucial role in the formation of the as-prepared structures, which leads to different band gap values. Ameen et al. [50] synthesized ZnO flower-like photocatalysts (E_g = 3.24 eV) which showed very high efficiency for crystal violet degradation under UV light irradiation. After 80 min of irradiation, about 96% was degraded. Mahmodiet al. [51] investigated the photocatalytic activity of ZnO on stainless steel support. The activity measurements were concerned with photoreduction of carbon dioxide in the presence of H_2, H_2O, and CH_4. It was noticed that TiO_2 has better photoreduction activity while the highest result for ZnO was achieved in the presence of CH_4 [51]. Li et al. [52] tested ZnO nanoparticles in the degradation reaction of methyl orange under UV light illumination. ZnO exhibited excellent degradation efficiency of methyl orange reached 97.84% after 30 min. Moreover, ZnO showed no significant loss of

photocatalytic activity during four repeated cycles [52]. Bismuth oxide with optical band gap value of 2.7 eV could be utilized as a visible-light-driven photocatalyst [79]. Iyyapushpam et al. prepared Bi_2O_3 by sol–gel method. Samples were calcined at two different temperatures (600 and 700°C), and the highest degradation efficiency was attained by semiconductor with higher crystallinity and specific surface area (sample calcined at 600 ◎C). The degradation percentage of methyl orange was found to be 76% [79].

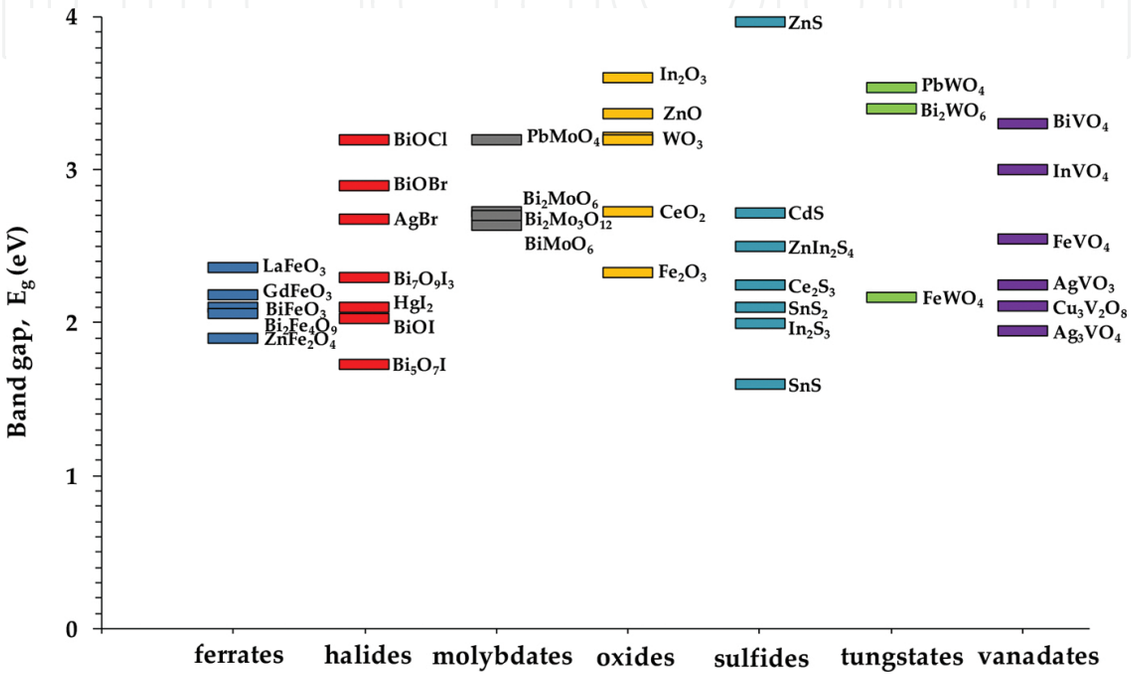

Figure 1. Band gap values for selected groups of photocatalyst collected based on the literature review.

Tungsten-based materials with a low band gap seemed to be promising candidate for the degradation of organic compound under visible light. For instance, Phattharanit et al. [128] obtained multi-layered flower-like Bi_2WO_6 by hydrothermal method and estimated activity of the powder in the degradation of rhodamine B under visible light. The results shown that after 360 min of irradiation, 88% of rhodamine B was degraded, which could be related to photosensibilization of semiconductor by dyes. In comparison, Saison et al. [129] synthesized Bi_2WO_6 with the band gap equals 2.9 eV and measured photocatalytic efficiency for Bi_2WO_6 and TiO_2. They observed relatively low activity of Bi_2WO_6 during rhodamine B and stearic acid degradation process under visible light. After calculation of the band diagram, Saison et al. explained that bismuth tungstate has inadequate band positions resulted in rapid recombination of excited pairs because electrons are not able to react with dioxygen.

Among the vanadates, $BiVO_4$ paid much attention because of the stability, nontoxicity, and relative high activity under the visible irradiation. In the most of the published papers, the photocatalytic activity of $BiVO_4$ was measured on model reaction of rhodamine B degradation [145–152]. Lin et al. [145] synthesized $BiVO_4$ (E_g = 2.36 eV) by simple hydrothermal

http://dx.doi.org/10.5772/62583

method. After 180 min of visible light illumination, 100% of rhodamine B (λ >420 nm) was degraded. The stability was evaluated during four cycles, which indicated no significant decrease in photocatalytic activity [145]. Tan et al. [148] synthesized $BiVO_4$ powders by hydrothermal method. By the manipulation of reaction condition, different hierarchical structures such as octahedron, decahedron, spherical, and polyhedral were obtained [148]. The influence of pH values on the crystalline phase and morphology of the $BiVO_4$ powders was examined. The highest visible light photocatalytic activity for the rhodamine B degradation was achieved by sample prepared at pH 7.81 with specific surface area equals 5.15 m^2 g^{-1}. Lin et al. [145] also observed high activity of fishbone-like $BiVO_4$ for RhB degradation. The band gap around 2.36 eV was estimated from UV–Vis spectra. After 180 min irradiation, 100% of dye was removed.

Recently, encountered research about silver halides provides information about excellent activity, however, suffers by very low stability of AgX, which radically limited potentially reuse and application [38]. On the other hand, majority of the bismuth oxyhalides described in literature are perceived as a wide band gap semiconductor with high stability. Guan et al. [21] compared properties of two different kinds BiOCl nanoplates and ultrathin nanosheets. They indicated that these powders varied in band gap value, for BiOCl nanoplates E_g reached 3.25 eV while for nanosheets 3 eV. The higher photocatalytic activity for the degradation of RhB was observed in the case of ultrathin BiOCl. This phenomenon was explained by the creation of different defects which are formed after reducing the thickness of the nanosheets to the atomic scale [21]. Xiao et al. [35] prepared $Bi_7O_9I_3$ microsheets using simple microwave heating route. The degradation of bisphenol A induced *via* visible light irradiation was investigated. After 60 min of irradiation, almost 100% of bisphenol A was degraded. The reaction rate constant of the optimal sample was over 16 times greater than that of TiO_2-P25. $Bi_7O_9I_3$ microsheets revealed high mineralization capacity of bisphenol A and good stability during the recycle tests, implying a promising forecast in the industrial application of the photodegradation of organic pollutants. The mechanism analyses conducted by LC–MS suggested that the degradation of bisphenol A under visible light irradiation occurred predominantly by direct holes, and the main detected intermediates were hydroquinone and methyl 4-hydroxybenzoate [35].

Ferrates can be specified as a semiconductor with narrow band gap. There are several synthesis methods described in the literature used for ferrate preparation such as hydrothermal [11, 13, 14, 17], microwave hydrothermal [15], microwave [16], solid-state reactions [12], and solution combustion method [18]. These photocatalysts possess superior properties, and therefore, they seemed to allow their use in environmental purification. Due to magnetic properties of ferrates, they can be easily separated from reaction suspension. Shahid et al. reported high photocatalytic activity of $MgFe_2O_4$ in the degradation of methylene blue under UV (350 nm) and visible light (λ > 420 nm). In comparison with ferrate, TiO_2-P25 exhibited poor photocatalytic activity under visible light; after 50 min of irradiation, only 10% of dye was decomposed, whereas in the presence of $MgFe_2O_4$ even 95% of MB was degraded [12]. Tang et al. indicated that $LaFeO_3$ with band gap equals 2.36 eV and strong visible light absorption exhibited much higher activity in the MB degradation than

TiO_2-P25 [16]. Li et al. [11] have examined activity of $GdFeO_3$ in the degradation of 4-chlorophenol under visible light irradiation ($\lambda > 420$ nm). After 5 h of illumination, only 20% of 4-chlorophenol was removed by TiO_2-P25, while almost 85% was degraded over $GdFeO_3$. That obtained $GdFeO_3$ microspheres have characterized by broad absorption in visible light region and quite well photocatalytic stability after fifth run [11].

According to the literature data, many other groups of semiconductors are also used in heterogeneous photocatalysis, such as tantalates, titanates, molybdates, niobates, selenides, phosphates, stannate, carbonate, germanate, and cobaltites. Most of tantalate- and titanate-based materials can be activated only *via* UV light due to generally wide band gap, which can reached even 5.05 eV [167–169]. Nevertheless, it has been reported that these photocatalysts exhibited high activity which may be attributed to crystal structure of perovskites. Liang et al. [47–49]. Microcrystalline $AgNbO_3$ was synthesized by Wu et al. [47] by sol–gel method. The photocatalyst has proved to be stable for all recycle experiments. However, $AgNbO_3$ has shown high activity only for the decomposition of methylene blue and rhodamine B, and for 4-chlorophenol and methyl orange, there was no obvious drop of contaminants concentration. Bismuth niobate prepared by a facile hydrothermal route showed very good visible-light-induced performance for the removal of nitrogen monoxide [48]. It has been shown that the activity results of bismuth niobate are better than that for C-doped TiO_2, $InVO_4$, and BiOBr nanoplates [48]. Promising properties have been noticed also for molybdate-containing materials such as Bi_2MoO_6 with interesting layered perovskite structure [40]. Sun et al. [40] tested Bi_2MoO_6 with nanoplate like morphology prepared *via* hydrothermal method. The photocatalytic performance was evaluated by the degradation of rhodamine B and phenol under environment-friendly blue light emitting diode ($\lambda = 465$ nm) irradiation. They have found that after 30 min of illumination, almost 100% of rhodamine B was degraded, while in the presence of TiO_2-P25, only several percent of dye was removed even with addition of H_2O_2. Phenol was chosen as another model substance in order to exclude the influence of photosensitization. They have examined synergistic effect of photocatalysts and H_2O_2 for the phenol degradation. After 2 h of irradiation, the amount of phenol decreased up to 8% in over Bi_2MoO_6. They have concluded that Bi_2MoO_6 with narrow energy gap is able to respond directly to blue light emitting diode in contrast to TiO_2-P25 [40]. Bi et al. [41] have investigated the stability of Bi_2MoO_6, and during five-cycle experiments, they have not observed any obvious decrease in photocatalytic activity for rhodamine B degradation. Hipolito et al. [46] prepared bismuth molybdate photocatalysts using co-precipitation method. The activity of so obtained $Bi_2Mo_3O_{12}$ was further investigated for the removal of nitric oxide under UVA light irradiation. In comparison with Bi_2MoO_6 with a band gap equals 2.44 eV, the $Bi_2Mo_3O_{12}$ ($E_g = 2.7$ eV) turned out to be more active reaching around 30% more of NO removal. This dispersion of results could be attributed to higher surface area of $Bi_2Mo_3O_{12}$ and its abundant adsorption sites for NO adsorption [46].

Summarizing, it is possible to find several photocatalysts which provide better light-harvesting performance than TiO_2, and it is assumed that they can be good replacement of TiO_2. Unfortunately, there is still lack of precise research related to possibility of reuse the powders. It is

http://dx.doi.org/10.5772/62583

needed to search new materials which will be environmental friendly, resistant to photocorrosion, and will not dissolve in water; otherwise, toxic metals and compounds such as Cd, Pb, or semiconductor sulfides will be useless for practical application. Most of the current research based on degradation of dyes, which can act as an organic semiconductor and participate in charge transition into CB under visible light irradiation. Therefore, the use of dye-photocatalysts system should be taken into consideration in the process of sewage treatment. Also, it should be noticed that the examination of activity in the degradation compounds such as 4-chlorophenol under UV light must be consider due to sensitivity to photolysis. Furthermore, results from the photolysis should be always placed with actual photocatalytic activity in order to make a reasonably comparison. There is still need for the standardization of photocatalytic measurements by utilizing the identical test equipment, photocatalysts dosage, kind and concentration of model compound, and other experiments condition, which allow making proper worldwide comparison of photocatalytic results.

Group	Semiconductor, Eg (eV)	Model pollutant	Irradiation range	Ref.
Antimonate	$GaSbO_4$ (3.7)	Acetone, salicylic acid	UV	[5]
	$AgSbO_3$ (2.6)	Rhodamine B	Vis	[6]
Carbonate	Ag_2CO_3 (2.46)	Rhodamine B, methyl orange, methylene blue	Vis	[7]
	$(BiO)_2CO_3$ (3.09–2.67)	Rhodamine B	UV	[8]
Cobaltites	$LaCoO_3$ (n/a)	Methyl orange	Vis	[9]
	La1–xBaxCoO_3 (2.80–2.21)	Formalachite green	Vis	[10]
Ferrate	$GdFeO_3$ (1.97–2.18)	4-Chlorophenol	Vis	[11]
	$MgFe_2O_4$ (n/a)	Methylene blue	Vis	[12]
	$BiFeO_3$ (2.1)	Rhodamine B	Vis	[13]
	$Bi_2Fe_4O_9$ (1.94–2.06)	Methyl orange	Vis	[14, 15]
	$LaFeO_3$ (2.36)	Methylene blue	Vis	[16]
	$ZnFe_2O_4$ (1.9)	Rhodamine B	Vis	[17, 18]
Germanate	$CeGeO_4$ (3.1)	Terephthalic acid	UV	[19]
	$ZnGa_2O_4$ (4.5)	Ethylbenzene, methyl orange, rhodamine B, methylene blue benzene, toluene	UV-Vis	[20]
Halides	BiOCl (2.87–3.2)	17 Alpha-ethinyl estradiol (EE2) and estriol, methyl orange, methylene green, rhodamine B, tetracycline hydrochloride	UV, Vis	[21–29]
	BiOBr (2.45–2.9)	Methyl orange, rhodamine B, tetracycline hydrochloride	UV, Vis	[22–24, 28, 30, 31]

Group	Semiconductor, Eg (eV)	Model pollutant	Irradiation range	Ref.
	BiOI (1.43–2.03)	Methyl orange, rhodamine B, tetracycline hydrochloride, 17 alpha-ethinyl estradiol (EE2), estriol	UV, Vis	[22–24, 32–34]
	$Bi_7O_9I_3$ (2.23–2.30)	Bisphenol-A	Vis	[35]
	Bi_5O_7I (1.73)	Rhodamine B	Vis	[36]
	HgI_2 (2.10)	Rhodamine B	Vis	[37]
	AgBr (2.58–2.68)	Methylene blue, methyl orange	Vis	[38, 39]
Molybdate	Bi_2MoO_6 (2.51–2.73)	Phenol, rhodamine B	Vis	[40, 41]
	$BiMoO_6$ (2.64)	Phenol, ibuprofen, rhodamine B	Vis	[42, 43]
	$PbMoO_4$ (3.1–3.2)	Methyl orange, rhodamine B , indigo carmine, orange G	UV, Vis	[44, 45]
	$Bi_2Mo_3O_{12}$ (2.73–2.70)	Nitric oxide	UV	[46]
Niobate	$AgNbO_3$ (2.9)	4-Chlorophenol, methyl blue, methyl orange, rhodamine B	Vis	[47]
	Bi_3NbO_7 (2.89)	Nitrogen monoxide	Vis	[48]
	$SnNb_2O_6$ (2.3–2.6)	Rhodamine B, methyl orange, malachite green	UV, Vis	[49]
Oxides	ZnO (2–3.37)	4-Chlorophenol, alizarin red S, CO2 reduction, hexane, methylene blue, reactive brilliant red K-2BP, methyl orange, rhodamine B, thionine, estrone, H2O2 generation, yellow 15	UV, UV-Vis	[50–70]
	ZrO_2 (n/a)	Direct Red 81 victoria Blue	UV-Vis	[71]
	WO_3 (2.4–3.21)	CO_2, CR, methyl blue, methylene blue, Orange II, rhodamine B	UV, Vis	[72–77]
	In_2O_3 (3.6)	Perfluorooctanoic acid	UV	[70]
	a-Fe_2O_3 (2.33)	Methylene blue	Vis	[78]
	Bi_2O_3 (1.3–2.73)	Cr(VI], aldehydes, congo red, rhodamine B, methyl orange	UV, Vis	[79–82]

Group	Semiconductor, Eg (eV)	Model pollutant	Irradiation range	Ref.
	CeO_2 (2.81–3.2)	4-Nitrophenol, indigo carmine, AO7, methylene blue, rhodamine B	UV, Vis	[83–86]
	Cu_2O (n/a)	Methyl orange	Vis	[87]
	Ga_2O_3 (n/a)	Methyl orange, rhodamine B	UV	[88]
	Nb_2O_5	Rhodamine B	UV, Vis	[89]
Phosphates	Ag_3PO_4 (2.35–2.47)	Bisphenol A, rhodamine B	Vis	[90–92]
	$BiPO_4$ (3.35–4.4)	Benzene, rhodamine B	UV	[93, 94]
selenides	ZnSe (2.9)	Methylene blue	Vis	[95]
Stannates	$CdSnO_3$ (4.4)	Benzene	UV	[96]
	Zn_2SnO_4 (n/a)	Reactive Red 141	Sunlight	[97]
	$ZnSnO_3$ (3.34)	Methylene blue	UV-Vis	[98]
Sulfides	CdS (2.1–2.5)	Methyl orange, methylene blue, methylene blue, rhodamine B	UV, Vis	[99–104]
	ZnS (3.37–3.97)	2, 4-Dinitrophenol, dinitrobenzene methylene green, rhodamine B, methyl orange	UV	[105–108]
	SnS_2 (2.1–2.25)	Methyl orange phenol, rhodamine B	Vis	[109–111]
	In_2S_3 (1.89–2.0)	DNA purine bases, formic acid, hydrogenation of 4-nitroaniline	UV, Vis	[112, 113]
	SnS (1.6–1.3)	Methylene blue	Vis	[114]
	Bi_2S_3 (n/a)	Methyl orange rhodamine B	UV, Vis	[115, 116]
	Ce_2S_3 (2.1)	Nitrobenzene reduction	UV, Vis	[117]
	$ZnIn_2S_4$ (2.72–1.92)	Benzyl alcohol	Vis	[118]
	$CdIn_2S_4$(n/a)	Inactivation of *Escherichia coli*	Vis	[119]
	$ZnIn_2S_4$ (n/a)	Methyl orange	Vis	[120]

Group	Semiconductor, Eg (eV)	Model pollutant	Irradiation range	Ref.
	$CdIn_2S_4$(n/a)	Methyl orange	Vis	[121]
Tantalates	$Sr_{0.25}H_{1.5}$ Ta_2O_6 H_2O (4.9)	Benzene oxidation	UV	[122]
	β-$BiTaO_4$ (2.45–2.65)	Methylene blue	Vis	[123]
	$Ba_4Ta_2O_9$ (5.05)	Methyl orange	UV	[124]
Titanate	$K_2Ti_6O_{13}$ (3.06–3.48)	Methyl orange	UV	[125]
	$FeTiO_3$ (2.54–2.58)	Rhodamine B	Vis	[126]
	$BaTiO_3$ (n/a)	Rhodamine B	Vis	[127]
Tungstates	Bi_2WO_6 (2.48–3.4)	2,4-Dichlorophenoxyacetic acid, methylene blue, rhodamine 6G, rhodamine B, tetracycline	UV, Vis	[128–139]
	$FeWO_4$ (2.17 eV)	Methyl orange	UV-Vis	[140]
	$SrWO_4$ (n/a)	Rhodamine B, rhodamine 6G	UV	[141]
	$Na_4W_{10}O_{32}$ (n/a)	Coumarin propan-2-ol	UV	[142]
	$NiWO_4$ (n/a)	Methylene blue	Vis	[143]
	$PbWO_4$ (3.54)	Acid orange II	UV	[144]
Vanadates	$BiVO_4$ (1.85–3.3)	Blue, ciprofloxacin, methylene phenol, rhodamine B	UV, Vis	[145–158]
	$AgVO_3$ (2.11–2.25)	Bisphenol A, rhodamine B	Vis	[159]
	Ag_3VO_4 (1.95)	Rhodamine B	Vis	[160]
	$InVO_4$ (2.4–3.0)	Ciprofloxacin, methylene blue, rhodamine B	Vis	[161–163]
	$FeVO_4$ (2.02–2.55)	Phenol	UV-Vis	[164]
	$Cu_3V_2O_8$ (2.11–2.05)	Methyl orange	Vis	[165]

Table 1. Selected representative photocatalysts and model substances used for activity measurements.

3. Single-semiconductor photocatalysts for water splitting

Photocatalytic water splitting, which is a process of decomposition of water into hydrogen and oxygen, is a promising method for obtaining clean and renewable energy. When light with an energy equivalent or greater than band gap of the semiconductor photocatalysts is irradiated,

http://dx.doi.org/10.5772/62583

the electrons in the valence band are excited into the conduction band. The excitation of electrons creates holes in the valence band. These photogenerated electrons and holes trigger the redox reaction [170]. There are three main steps of photocatalytic water splitting: (1) The photocatalyst absorbs photon energy and electron–hole pairs are generated in the bulk; (2) the photo-excited charge carriers should separate and migrate to the surface with minimal recombination; and finally, (3) the free charge carriers triggers the oxidation and reduction reaction respectively at the surface, that is, the electron reduces H_2O to H_2 and the hole oxidized H_2O to O_2, respectively.

The production of hydrogen using a particulate photocatalyst has been examined by various research groups since 1972 and since that time scientists are trying to obtain the most efficient combination of semiconductors which will give payable level of hydrogen recovery [171]. In recent years, many various types of homogeneous and heterogeneous photocatalysts have been developed and intensively analyzed. Summary of studied heterogeneous photocatalysts used for water-splitting process are presented in **Table 2**. In fact, heterogeneous photocatalysis received lately more attention because of wider application scale. There is no single photocatalyst which can meet all the requirements to proceed efficient water-splitting process for H_2 production. The success is not only in careful selection of semiconductor photocatalysts but also their optimal surface structures. Additionally, a suitable band gap, matching energy band for H_2 and O_2 evolution, high quantum efficiency and stability are also important. The main task of scientists is to develop the composition of semiconductor materials, which will carry out suitable optical absorption, reduction, and oxidation abilities and increase efficiency in solar energy conversion [197]. It is thought that co-catalyst components such as Pt, Ni, Rh, and Ru can promote H_2 evolution because of their lower over potentials, while they are also active for the oxygen reduction reaction (ORR), which corresponds to the reverse of the water-splitting reaction [36]. Positive water splitting was also observed in the presence of co-catalysts such as Pt, Pd, and Rh or a metal oxide such as NiO, RuO_2, and Cr_2O_3, which are loaded onto the photocatalyst surface to produce active sites for water reduction reaction [171]. Following the assumption of water-splitting process for hydrogen production, we chose these examples, which demonstrate the best perspectives.

Following the idea of development of better photocatalysts for water splitting in visible light spectrum, we chose the most promising examples by comparing energy band gaps and hydrogen production rate, not considering TiO_2 photocatalysts. The apparent quantum yield (AQY) for the production of hydrogen and oxygen gas can be estimated by the following Equation (1):

$$\mathrm{AQY}(\%) = \frac{\text{number of reacted electrones}}{\text{number of incident photons}} \times 100 \tag{1}$$

Liao et al. [180] conducted water-splitting process using cobalt oxide particles. The photocatalysts were obtained from nonactive CoO micropowders with two distinct methods —femtosecond laser ablation and mechanical ball-milling. Water-splitting experiments were performed in air-tight flasks with CoO nanoparticles suspended in neutral water. Generation

of hydrogen and oxygen was measured by a gas chromatograph (GC) equipped with a thermal conduction detector (Gow-Mac). High photocatalytic activity of the nanoparticles was analyzed by electrochemical impedance spectroscopy (SRS residue gas analyser, RGA200), which comes from a significant shift in the position of the band edge of the material with regard to water redox potential. The conduction band of CoO micropowder is located below the hydrogen—evolution potential what leads to inactivity in water splitting process. A mass spectrometer was also used to identify isotope gas species from water splitting. Received CoO nanoparticles can decompose pure water under visible light irradiation without any co-catalysts or sacrificial reagents with the hydrogen production assessed for 71,429 μmol/h g^{-1} [180].

Twinned $Cd_{0.5}Zn_{0.5}S$ anisotropic nanocrystals (called nanorods) with controllable aspect ratios and a high proportion of long-range ordered twin planes were investigated by Liu et al. [195]. Between the planes in the crystal, the zinc–blende (ZB) and wurtzite (WZ) were generated. The TEM image revealed that nanorods consisted of a high density of stacking faults with parallel distribution, which were coherent twin boundaries. During the process between the segments of ZB and WZ, the type II staggered band was created which in particular dimension cause the generation of myriad homojunctions. This formation leads to photocatalytic hydrogen production with a remarkable QE of 62% and 25,800 μmol/h g^{-1}. Different combinations of the same elements were investigated by Li et al. [194], where the solid solution of $Zn_{1-x}Cd_xS$ was analyzed. Obtained structures characterized with a small crystallite size and precise band structure. The photocatalytic hydrogen production experiment was performed at ambient temperature and atmospheric pressure, using 350 W xenon arc lamp through a UV cut-off filter ($\lambda > 400$ nm). Study revealed that sample containing $Zn_{0.5}Cd_{0.5}S$ is the most promising in terms of hydrogen production with the rate of 7420 μmol/h g^{-1}, which is much more than amounts produced with the pure CdS or ZnS samples.

Group	Semiconductor, Eg (eV)	Irradiation range(nm)	H_2 production rate (μmol/h g^{-1})	O_2 production rate (μmol/h g^{-1})	Apparent quantum yield (%)	Ref.
Sulfides	CdS (2.4)	λ>420	25	n/a	n/a	[172]
	$CaIn_2S_4$(1.84–168)	λ>420	2.64	n/a	n/a	[173]
	Sb_2TiS_5 (1.87)	UV	10.4	n/a	n/a	[174]
	$(CuAg)_{0.15}In_{0.3}Zn_{1.4}S_2$ (2.72–1.92)	λ>420	1750	n/a	12.8	[175]
	$ZnIn_{2.3}S_{4+y}$ (4.894)	λ>420	363	n/a	n/a	[176]
	Cu_3SnS_4(1.38)	λ>420	1100	n/a	3.9	[177]
	$Mn_{0.24}Cd_{0.76}S$(2.28)	λ>420	10,900	n/a	9.5	[178]
Oxides	Ta_2O_5 (3.9)	λ>420	7100	n/a	n/a	[179]

http://dx.doi.org/10.5772/62583

Group	Semiconductor, Eg (eV)	Irradiation range(nm)	H_2 production rate (μmol/h g^{-1})	O_2 production rate (μmol/h g^{-1})	Apparent quantum yield (%)	Ref.
	CoO (2.6)	λ>420	71,429	35 714	5	[180]
	Fe_2O_3 (2.3)	λ>420	n/a	3	n/a	[181]
Vanadates	$InVO_4$(3.0)	λ>420	14.16	n/a	n/a	[182]
	$Ag_2Sr(VO_3)_4$(2.4)	λ>420	n/a	8,1	n/a	[183]
	$Sr(VO_3)_2$ (2.7)	λ>420	n/a	12	n/a	[183]
Halides	LaOF (4.7)	UV	27	n/a	n/a	[184]
Tantalites	$NaTaO_3$ (4.1)	UV	3106	n/a	n/a	[185]
	$Cd_2Ta_2O_7$ (3.35)	UV	173	86.3	n/a	[186]
Ferrates	$GaFeO_3$ (2.02-2.18)	λ>395	289	n/a	n/a	[187]
	$LaFeO_3$ (2.07)	λ>420	3315	n/a	n/a	[188]
	$ZnRh_2O_4$(1.2-2.2)	UV, Vis	500	n/a	27	[189]
	$NiFe_2O_4$ (1.7)	λ>420	1.97	n/a	0.07	[190]
	Ta_3N_5 (2.08)	λ>420	410	n/a	–	[191]
	$ZnIn_2S_4$(2.59-2.83)	λ>420	220.45	n/a	13.16	[192]
	$Bi_{0.5}Na_{0.5}TiO_3$ (2.82-2.92)	UV-Vis	324.5	n/a	3	[193]
	$Zn_{0.5}Cd_{0.5}S$ (2.45)	λ>420	7420	n/a	9.6	[194]
	$Cd_{0.5}Zn_{0.5}S$ (2.62)	λ>420	25,800	n/a	62	[195]
	$K_{0.5}La_{0.5}Bi2Ta_2O_9$/ $K_{0.5}La_{0.5}Bi_2Nb_2O_9$ (3.22-3.9)	UV	5.9–531	3.4 – 182	n/a	[196]

Table 2. Non-TiO_2 single photocatalysts for water splitting in UV/visible light spectrum.

Solid solutions of $Mn_{1-x}Cd_xS$ were fabricated by hydrothermal route in low temperature (130°C) by Liu et al. [178]. The H_2 evolution from water was performed under 300 W Xe lamp. 0.025 g of powder photocatalyst was dispersed in a pyrex cell with aqueous solution of 0.1 M Na_2S and 0.5 M Na_2SO_3. The characterization of samples revealed that with growing value of *x*, the rate of hydrogen increases. The highest value of H_2 production presented $Mn_{0.24}Cd_{0.76}S$ which in fact exceeds rate for pure CdS. The procedure was continued, and after third turn, the amount of H_2 decreased, what can be the result of consumption of the sacrificial agents—Na_2S and Na_2SO_3. The examined solution shows good photocatalytic stability and anti-

photocorrosion capability during water-splitting reaction what can be a promising discovery for the future. There are some examples of semiconductors which generate smaller amount of hydrogen than compounds described above; however, it still have potential for further studies in water-splitting area. $ZnRh_2O_4$with rate of hydrogen production of 500 μmol/h g^{-1} was studied by Takimoto et al. [189]. The measurements were conducted under monochromatic light and full Xe light lamp in wide range of wavelengths ($400 < \lambda \leq 770$ nm) with an intensity of 10 μW/cm^2. The amount of hydrogen produced is much less than in case of other presented semiconductors, but it is extraordinary because of a high efficiency yield (12%) at a wavelength of $\lambda = 770$ nm. The study revealed that this photocatalyst should be deeper investigated mainly because of possible usage in a wide range of light spectrum both visible and infrared light what is quite unique [189].

The overall compilation of already conducted experiments shows that there is a big potential for hydrogen production in photocatalytic water splitting in visible light range. The values of energy band gap indicate that non-TiO_2 single photocatalysts should be good candidates used in hydrogen production process without light limitations. The most promising results were obtained for different combinations of Cd composite what can lead to further studies in this particular area. Unfortunately, it is clear that single photocatalysts are not as efficient as should be expected. This is the reason why attention of researchers has been moved to more promising topics as the binary and ternary compounds or doping processes. Moreover, the demonstration of the simultaneous evolution of H_2 and O_2 is extremely difficult in the two-step water-splitting system because backward reactions easily proceed over each photocatalyst.

4. Binary composite photocatalysts

There are number of different types of photocatalytic materials, which are inefficient or not active during the light-mediated process of pollutants degradation. Various methods are used to improve the oxidation ability of photocatalysts in purification systems, such as doping with nonmetal ions, rare-earth metals, noble metals and transition metal ions, surface modification, dye sensitizing [198]. Among them, enhancing the photocatalytic activity can be achieved by coupling single semiconductors in composites.

Synthesis of new 3D semiconductor composites creates the opportunity to use materials with lower energy activation as a photocatalysts. Furthermore, application of the composite structures can lead to photocatalysts activated by low powered and low cost irradiation sources (such as LEDs or black fluorescent UV lamps) and can be used both in air and water purification systems. Therefore, it is important to develop convenient, low-cost, and environmental-friendly methods to synthesize high-quality photocatalysts.

Nowadays promising idea based on combining wide band gap semiconductors with narrow band gap materials. The narrow band gap photocatalyst can be excited in visible light region. The photogenerated holes and electrons can be transported to the wide band gap semiconductor and photo-excited with lower energy transfer. Furthermore, the nanocomposites materials exhibit improved quantum efficiency. Therefore, composites with narrower band

http://dx.doi.org/10.5772/62583

gap semiconductors have been developed to extend the photo-absorption range, facilitate the separation of the photo-induced carriers, and extend the activity into the visible light region. A composite of two photocatalysts with surface contact formed a heterojunction which limits the electron transfer. There are three main processes which may lead to consumption of the photo-induced electrons: (*i*) volume recombination (recombination with produced holes inside the photocatalyst), (*ii*) surface recombination (reaction with spices on surface of the particle, and (*iii*) the H_2 production as a result of reaction with protons.

4.1. Photo-excitation mechanisms of binary composites

In general, there are three different mechanisms of binary composite photo-excitation under ultraviolet and visible light. Most of the current research is focused on efficiently suppression of the recombination processes. Summary of studied composites and possible mechanisms of photo-excitation (named mechanism A, B, and C) are presented in **Table 3**. During the irradiation, both photocatalysts can be excited with photogenerated charge carriers depending on the band gap energy (E_g). Usually under visible light irradiation, the electrons produced in narrow band gap semiconductor (named semiconductor A) with less positive conduction band (CB) can be transferred quickly to the more positive CB of the photocatalyst with the wider band gap (semiconductor B). In the other hand, the photo-excited holes from semiconductor B could be shifted easily into the valence band (VB) of the semiconductor A. The each position of conduction and valence band in photocatalysts according to the mechanism A is presented in **Figure 2a**. The $Ag_3PO_4/ZnFe_2O_4$ composite was synthesized by Chen et al. *via* a solvothermal-liquid phase deposition method [230]. The photocatalytic activity test was performed as a 2,4-dichlorophenol degradation under visible light irradiation. During the process using $Ag_3PO_4/ZnFe_2O_4$ with mass ratio 9:1, 95% of the pollutant was decomposed after 70 min of irradiation (two and three times higher than result for single photocatalyst). It was found that the conduction and valence band of $ZnFe_2O_4$ is more negative than CB and VB of Ag_3PO_4. Structure formation of $Ag_3PO_4/ZnFe_2O_4$ material resulted in expanding the spectral responsive range of Ag_3PO_4. High-effective photocatalyst under Vis light was obtained by combining the single $BiVO_4$ with $FeVO_4$ [222]. The heterojunction composite photocatalysts was stable in photocatalytic removal of metronidazole in aqueous phase. Moreover, enhanced oxidation properties resulted from the fast transfer of photogenerated charge carriers. The optimal weight ratio in Ag_3PO_4/BiOBr composite was equal to 0.7. The process of energy bias generation at heterojunction plays significant role in electron and hole pair transfer. The rate of removal rhodamine B under visible light was maintained at 95% after 6 recycling processes [224].

In view of the internal field between semiconductors, in some composites used for photodegradation under visible light, only electron transfer exists without hole migration in the valence band (the process is named mechanism B, see **Figure 2b**) [199, 213, 214, 218, 219]. Xu et al. [213] synthesized CdS/MoS_2 composite active under visible irradiation range. The favorable heterojunction between CdS and MoS_2 extended lifetime of the charge carriers [213, 214]. The same type of mechanism was observed for CdS/SnO_2 photocatalyst where electrons shift from cadmium sulfides conduction band to the thin oxides band [199]. Consequently, the charge carriers in junction between semiconductors were effectively separated *via* one-step process.

All types of described mechanisms (mechanism A, B, and C) are caused by the presence of heterojunctions among different semiconductors that enhance the separation of the photo-generated electron–hole pairs, hindering their recombination.

Whereas, under the ultraviolet light illumination, both semiconductors simultaneously or the semiconductor with wider band gap in the composite could be excited. The mechanism of photo-excitation in binary composites was investigated by Hamrouni et al. Two photocatalysts: $ZnO/ZnWO_4$ and ZnO/SnO_2 prepared by a facile sol–gel method were examined in the photocatalytic decomposition of 4-nitrophenol under ultraviolet light range [200]. It was found that the local heterojunction between the photocatalysts pair facilitates the separation of the photogenerated e^-/h^+ pairs (mechanism C, see **Figure 2c**). A photocatalysts with enhanced electron–hole separation and excellent photocatalytic performance was investigated by Duo et al. [215, 217]. The methyl orange solution and Rhodamine B were used as a model substance in degradation under simulated sunlight. Both composites $BiPO_4/BiOCl$ and $BiPO_4/BiOBr$ exhibited significantly higher activity in dyes elimination than single semiconductors [216, 217].

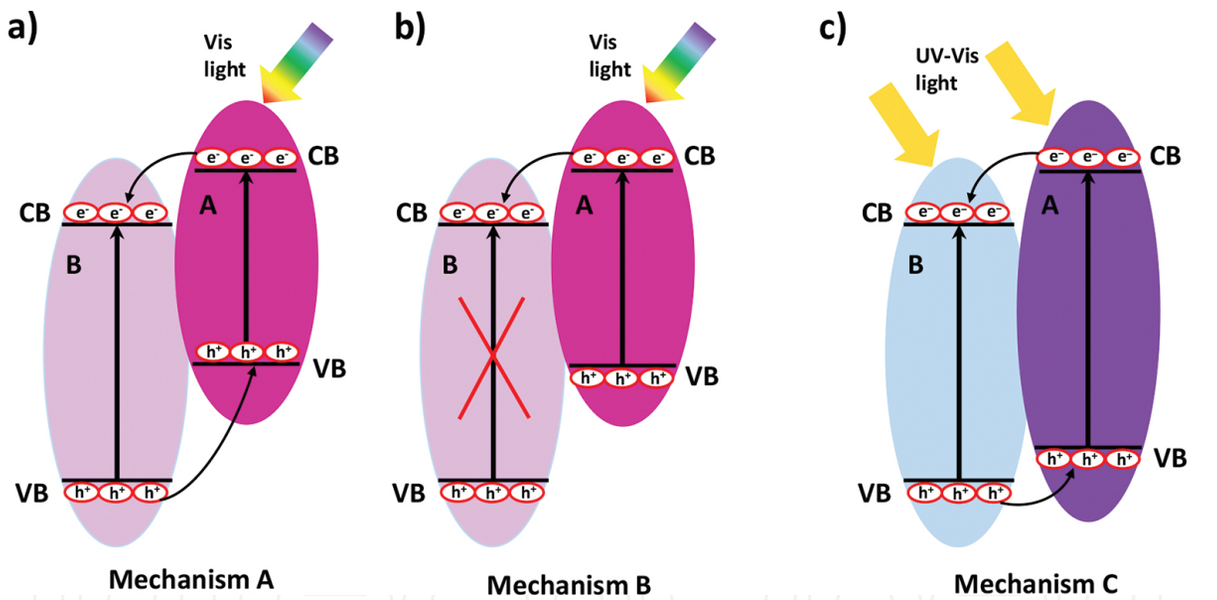

Figure 2. Possible mechanism of semiconductors composite photo-excitation: (a) Mechanism A under UV–Vis light, (b) Mechanism B under Vis light, and (c) Mechanism C under Vis light.

Semiconductor A	Semiconductor B	Irradiation range	Excitation mechanism	Ref.
CdS (2.17)	SnO_2 (3.3; 3.55)	Vis	Mechanism C	[199]
ZnO_2 (3.2)		UV	Mechanism A	[200]
ZnO_2 (3.2)	$ZnWO_4$ (3.14)	UV	Mechanism A	[200]
ZnO_2 (3.2)	Bi_2O_3 (2.8; 2.38; 2.75; 2.89)	UV	Mechanism A	[201]
$NaBiO_3$ (2.36)		Vis	Mechanism B	[202, 203]

Semiconductor A	Semiconductor B	Irradiation range	Excitation mechanism	Ref.
$BaTiO_3$ (3.18)		UV	Mechanism A	[204]
$NaBi(MoO_4)_2$ (3.08)		Vis	Mechanism B	[205]
Bi_5O_7I (3.13)		Vis	Mechanism B	[206, 207]
Bi_2O_3 (2.9)	Bi_2WO_6 (2.8; 3.1; 2.97)	Vis	Mechanism B	[208]
$ZnWO_4$ (3.75)		UV-Vis	Mechanism A	[209]
CeO_2 (2.58)		UV-Vis	Mechanism A	[210]
$Bi_{12}TiO_{20}$ (2.57		UV-Vis	Mechanism A	[211]
CdS (2.22)	Bi_2MoO_6 (2.8)	Vis	Mechanism B	[212]
CdS (2.25)	MoS_2 (1.75)	Vis	Mechanism C	[213, 214]
BiOBr (2.62)	$BiPO_4$ (4.16; 3.83; 4.11)	Sunlight, Vis	Mechanism A, Mechanism C	[215, 216]
BiOCl (3.12)		Sunlight	Mechanism A	[217]
Bi_2MoO_6 (2.53)		Vis	Mechanism C	[218]
Bi_2MoO_6 (2.71)	$BiIO_4$ (3.02)	Vis	Mechanism C	[219]
Cu_2O (2.5)	BiVO4 (2.0; 2.47)	Vis	Mechanism B	[220, 221]
$FeVO_4$ (2.05)		Vis	Mechanism B	[222]
$BiVO_4$ (2.49)	$Bi_4V_2O_{11}$ (2.22)	Vis	Mechanism B	[223]
Ag_3PO_4 (2.36)	BiOBr (2.74; 3.13; 2.76; 2.81)	Vis	Mechanism B	[224]
BiOI (2.45; 1.74; 1.72)		Vis	Mechanism B	[225–227]
BiOI (1.90)	WO_3 (2.60)	Vis	Mechanism B	[228]
WO_3 (2.68)	H_2WO_4 (2.45)	Vis	Mechanism B	[229]
$ZnFe_2O_4$ (1.88)	Ag_3PO_4 (2.44)	Vis	Mechanism B	[230]
Ag_3VO_4 (2.05)	Co_3O_4 (2.07)	Vis	Mechanism B	[231]
	$ZnFe_2O_4$ (1.90)	Vis	Mechanism B	[232]
$Ag_4P_2O_7$ (2.63)	AgBr (2.6)	Vis	Mechanism B	[233]
AgBr (2.64)	ZnO (3.0; 3.22; 3.3; 3.37; 3.26)	Vis	Mechanism C	[234–237]
Ag_2S (1.0)		Sunlight	Mechanism A	[238]
AgI (−)		Vis	Mechanism C	[239]
AgI (2.51)	Ag_2CO_3 (2.30)	Vis	Mechanism B	[240]
$SmCrO_3$ (2.7)	$Sm_2Ti_2O_7$ (3.2)	Sunlight	Mechanism A	[241]
In_2O_3 (2.90)	α-Fe_2O_3 (2.03)	Vis	Mechanism B	[242]

Table 3. Summary of studied composites and possible mechanisms of photo-excitation.

4.2. Ternary composite photocatalysts

Based on the literature data, it could be expected that ternary semiconductor composites provide an opportunity for multi(two)-photons excitation of photoactive materials with lower energy photons and utilization of heterojunction to drive electronic processes in the desired direction. Consequently, the selective photo-excitation of localized electronic states to gain better selectivity should be achieved [243].

The composite of $KTaO_3$–CdS–MoS_2 with different molar ratio was synthesized by Bajorowicz et al. [244] *via* hydrothermal method. The micromaterials were prepared under strictly controlled conditions of temperature and pressure depending on the material type. Hydrothermal method does not require a calcination step and is easy to carry out technological conditions. Various structures of the photocatalysts such as cubic, hexagonal, nanoleaf, and microspheres were obtained. Calcination at 500°C for 3 h and hydro/solvothermal mixed solutions method were used to combine single semiconductors. The highest phenol photodegradation (80% under UV–Vis and 42% under Vis light) was observed for the $KTaO_3$–CdS–MoS_2 at the 10:5:1 molar ratio. In the toluene oxidation process under ultraviolet light, the powder exhibit very good stability and efficiency during four measurement cycles (activity reached about 50%) [244]. A comparatively to SnO_2/ZnO/$ZnWO_4$ composites in this case probably a two-photon excitation occurs under UV–Vis irradiation [200, 244]. The $KTaO_3$/CdS/WO_3, $KTaO_3$/CdS/MoS_2, $KTaO_3$/CdSe/$SrTiO_3$ composites preparing by various route with different molar ratio were compare in photocatalytic degradation of gaseous toluene under ultraviolet light. The results suggest that the structure, morphology, and photoactivity depend on the type and molar content of additional semiconductors as well as on the preparation method. Samples prepared by one-pot hydrothermal synthesis had higher surface area. Unfortunately, the morphology was not well developed and crystal structures of each single semiconductor were not formed. In four subsequent cycles, the photoactivity using the $KTaO_3$/CdS/MoS_2 (10:5:1) ranged 60% after 60 min of irradiation [245]. Hong et al. found that highly enhanced photocatalytic activity is due to synergistic effects of heterostructured ZnS/CuS/CdS material which can improve light absorption and charge carriers flow. The photocatalyst was stable under applied conditions (under solar irradiation 1 kW/m^2, AM 1.5 G) in H_2-production from a water splitting. The optimum ratio of loading the Cu equal to 0.81 wt% and Cd equal to 14.7 wt% was selected. The authors believed that the solar light causes electron excitation and separation in CdS (because of relatively narrow band gap), and consequently, efficient separated carriers flow to CuS conduction band during the holes from the ZnS were transferred to the valence band of CdS. Additionally, enhancing the H_2 production may result from the interfacial charge transfer between valence band of ZnS and CuS and partial reduction of CuS to Cu_2S [246]. It was observed that for some composites (i.e., ZnO/AgBr/Ag_2CrO_4), two semiconductors are excited and act as electron donors for wider photocatalyst. Reduction processes of the pollutant occur in the conduction band of the electron acceptor, whereas the electron donors will responsible for the oxidation reactions on valence band [247]. On the other hand, other mechanism, where ZnO plays a role of electron donor, was observed for SnO_2/ZnO/$ZnWO_4$ composite [200]. The SnO_2/ZnO/$ZnWO_4$ composite was examined under UV irradiation in 4-nitrophenol degradation process. Generated

http://dx.doi.org/10.5772/62583

electrons in the conduction band of ZnO are shifted to those of SnO_2 and $ZnWO_4$; meanwhile, holes may be transferred from the valence band of SnO_2 and $ZnWO_4$ to that of ZnO. It was established that the elimination efficiency of a pollutant depends on adsorption level on the photocatalytic surface and ability to react with the photogenerated charge carriers. The amount of each semiconductors in the photocatalytic material determined the photocatalytic activity [200]. Enhanced photocatalytic activity in rhodamine B degradation process was observed for In_2O_3/AgBr/Bi_2WO_6 ternary composite (see structure on **Figure 3a**) [248]. Photocatalyst has exhibited higher activity under UV, visible, and simultaneous sunlight in comparison to single Bi_2WO_6 semiconductor, binary AgBr/Bi_2WO_6 material and pure P25. Proposed mechanism based on electrons transfer from In_2O_3 with the widest band gap to AgBr and consequently transition e^- from AgBr to Bi_2WO_6, which is semiconductor with the least negative CB in composite. The generated O_2^{*-} radicals in the conduction band plays a role in oxidation processes of pollutant. The produced holes (h^+) in the VB of semiconductors can oxidize the water molecules on the photocatalyst surface and leads to produce hydroxyl radicals (*OH) which are able to degrade dyes into CO_2 and H_2O (see **Figure 3b**.) [248]. A various materials are tested in different model photocatalytic reactions and under various conditions. Therefore, it is intricate to summarize and compare properties and photoactivity of new 3D structures. Some already investigated combinations of ternary composites are presented in **Table 4**.

Semiconductor I, Eg (eV)	**Semiconductor II, Eg (eV)**	**Semiconductor III, Eg (eV)**	**Irradiation range**	**Ref.**
ZnO (3.2)	AgBr (2.6)	Ag_2CrO_4 (1.8)	Vis	[247]
ZnO (−)	Ag_3VO_4 (2.1)	Fe_3O_4 (−)	Vis	[249]
ZnO (3.2)	AgI (2.8)	Fe_3O_4 (0.1)	Vis	[250]
ZnO	Ag_1	Ag_2CrO_4	Vis	[251]
SnO_2 (3.2)	ZnO (3.55)	$ZnWO_4$ (3.14)	UV	[200]
CdS (2.25)	PbS (1.2–1.5)	ZnO (3.36)	Vis	[252]
ZnS	CuS	CdS	Sunlight	[246]
Fe_3O_4 (−)	AgBr (−)	ZnO (3.2)	Vis	[253]
Fe_3O_4 (0.1)	SiO_2 (8.9)	Bi_2MoO_6 (2.71)	Vis	[254]
BiOBr (2.72)	SiO_2 (−)	Fe_3O_4 (−)	UV-Vis, Vis	[255]
Bi_2S_3	Bi_2O_3	$Bi_2O_2CO_3$	Vis	[256]
In_2O_3 (3.75)	AgBr (2.6)	Bi_2WO_6 (2.76)	UV, Vis, sunlight	[248]
Ag_2O	Ag_3VO_4	$Ag_4V_2O_7$	Vis	[257]
PdS (−)	CdS (−)	NiS (−)	Vis	[258]

Table 4. Compilation of ternary composites and photo-excitation irradiation range.

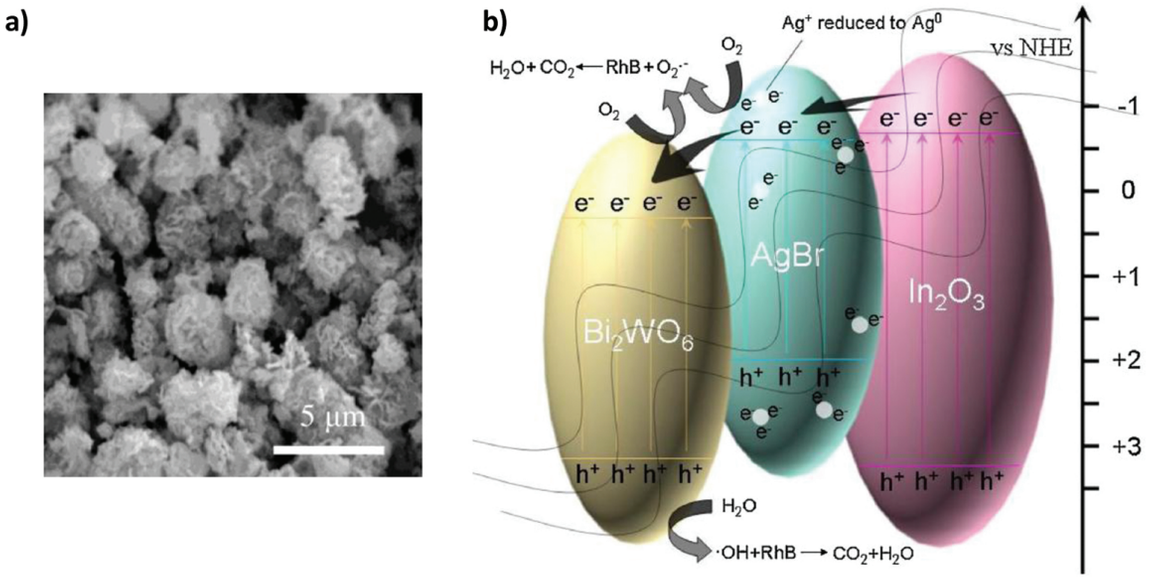

Figure 3. Ternary In_2O_3/AgBr/Bi_2WO_6 photocatalyst (a) Scanning Electron Microscope image, (b) Possible mechanism of photo-excitation in composite structure. Adapted with permission from Ref. [248].

Concluding the mechanism of photo-excitation of ternary composites, it is still not well understood. According to Serpone theory, photo-excitation of components A and B would be very efficient because the two nanomaterials are activated through their fundamental absorption band [243, 259]. There are some interactions which probably occur, while the irradiation excites photocatalyst. The process could be sophisticated and need further investigation.

5. Conclusions

Semiconductor photocatalysis affords a potential solution to the problems of energy shortages and environmental pollution. However, photo-efficiency of the most single semiconductors is limited because of the rapid electron–hole recombination. Therefore, the development of efficient visible-light-driven photocatalysts is a major challenge in this field. The photocatalytic activity of semiconductor photocatalysts depends on its physical and chemical properties, and additionally, depends on the recombination of photo-excited electrons and holes occurs at crystal lattice defects. Fortunately, the coupling of two or three semiconductors with different band gap values could improve the stability, necessary for practical applications and could extend the energy range used for excitation. Especially, the fabrication of a *p–n* junction is believed to be the most effective because of the existence of an internal electric field. Moreover, the hybrid photocatalyst can benefit from the synergistic effects such as enhanced light-harvesting ability, efficient photogenerated electron–hole separation, and improved photostability, and thus, the photoactivity is remarkably improved. However, it should be noted that the reason for the improvement of composite photocatalyst is not only due to the effects described above but also due to enhancement of surface acidity or alkalinity and the surface

http://dx.doi.org/10.5772/62583

population of OH groups, which can promote the adsorption of reaction substrates and facilities the generation of hydroxyl radicals (•OH), respectively.

Based on the literature data, it can be concluded that most of the photocatalytic investigations are focused on dyes oxidation (such as methyl orange, rhodamine B, methylene blue, and malachite green) as the model degradation process of pollutants. According to Ohtani recommendation, the use of organic dyes as a model compound for photocatalytic decomposition reaction, enabling the feasible determination of photocatalytic activity, especially using spectrophotometric analysis [260]. He indicated at least three reasons for its inappropriateness. One is that the dye molecules absorb photons, especially in the visible light range, and thus photo-excited electrons may be injected into photocatalyst particles as has been suggested by the action spectrum similar to the absorption spectrum of the dye. Another reason is that the absolute molar amount of dye contained in the reaction system can be much smaller than that of a solid photocatalyst. Since the photo-absorption coefficient of dyes is generally large, for example, $>10^5$ mol^{-1} L cm^{-1}, the concentration can be 10^{-5} mol L^{-1} and the absolute molar amount can be 10^{-6} mol when the volume of the solution is 100 mL. The third reason is that the mechanism of dye degradation is so complicated that efficiency of the photocatalytic reaction cannot be measured.

In this point of view, there are still few works investigated on the photoactivity of composite photocatalyst shows enhanced photocatalytic activity for water splitting and organic degradation except dyes. Additionally, to better understand the properties of semiconductor composites and their role in photocatalysis processes, novel preparation methods need to be developed. Moreover, photocatalytic mechanisms and relationships among the structures forming the composites, surface, and crystal properties and photocatalytic activity should be thoroughly investigated and clarified.

Acknowledgements

This work was supported by Ministry of Science and Higher Education (Contract No.: UMO-0132/IP2/2015/73) and National Science Center (Contract No.: UMO-2014/15/N/ST8/03753).

Author details

Martyna Marchelek, Magdalena Diak, Magda Kozak, Adriana Zaleska-Medynska and Ewelina Grabowska*

*Address all correspondence to: ewelina.grabowska@ug.edu.pl

Department of Environmental Technology, Faculty of Chemistry, University of Gdansk, Gdansk, Poland

References

[1] Chen C, Ma W, Zhao J. Semiconductor-mediated photodegradation of pollutants under visible-light irradiation. Chemical Society Reviews. 2010;39(11):4206–4219.

[2] Li K, An X, Park KH, Khraisheh M, Tang J. A critical review of CO_2 photoconversion: Catalysts and reactors. Catalysis Today. 2014;224:3–12.

[3] Ahmad H, Kamarudin S, Minggu L, Kassim M. Hydrogen from photo-catalytic water splitting process: A review. Renewable and Sustainable Energy Reviews. 2015;43:599–610.

[4] Qu Y, Duan X. Progress, challenge and perspective of heterogeneous photocatalysts. Chemical Society Reviews. 2013;42(7):2568–2580.

[5] Fu Y, Xue H, Qin M, Liu P, Fu X, Li Z. Nanocrystalline $GaSbO_4$ with high surface area prepared via a facile hydrothermal method and its photocatalytic activity study. Journal of Alloys and Compounds. 2012;522:144–148.

[6] Liu W, Liu X, Fu Y, You Q, Huang R, Liu P, et al. Nanocrystalline pyrochlore $AgSbO_3$: Hydrothermal synthesis, photocatalytic activity and self-stable mechanism study. Applied Catalysis B: Environmental. 2012;123:78–83.

[7] Dong H, Chen G, Sun J, Li C, Yu Y, Chen D. A novel high-efficiency visible-light sensitive Ag_2CO_3 photocatalyst with universal photodegradation performances: Simple synthesis, reaction mechanism and first-principles study. Applied Catalysis B: Environmental. 2013;134:46–54.

[8] Tang J, Zhao H, Li G, Lu Z, Xiao S, Chen R. Citrate/urea/solvent mediated self-assembly of $(BiO)_2CO_3$ hierarchical nanostructures and their associated photocatalytic performance. Industrial & Engineering Chemistry Research. 2013;52(35):12604–12612.

[9] Jung WY, Hong S-S. Synthesis of $LaCoO_3$ nanoparticles by microwave process and their photocatalytic activity under visible light irradiation. Journal of Industrial and Engineering Chemistry. 2013;19(1):157–160.

[10] Zhang C, He H, Wang N, Chen H, Kong D. Visible-light sensitive $La_{1-x}Ba_xCoO_3$ photocatalyst for malachite green degradation. Ceramics International. 2013;39(4): 3685–3689.

[11] Li X, Duan Z-Q. Synthesis of $GdFeO_3$ microspheres assembled by nanoparticles as magnetically recoverable and visible-light-driven photocatalysts. Materials Letters. 2012;89:262–265.

[12] Shahid M, Jingling L, Ali Z, Shakir I, Warsi MF, Parveen R, et al. Photocatalytic degradation of methylene blue on magnetically separable $MgFe_2O_4$ under visible light irradiation. Materials Chemistry and Physics. 2013;139(2):566–571.

[13] Wei J, Zhang C, Xu Z. Low-temperature hydrothermal synthesis of $BiFeO_3$ microcrystals and their visible-light photocatalytic activity. Materials Research Bulletin. 2012;47(11):3513–3517.

[14] Liu Y, Zuo R. Morphology and optical absorption of $Bi_2Fe_4O_9$ crystals via mineralizer-assisted hydrothermal synthesis. Particuology. 2013;11(5):581–587.

[15] Liu Z, Wu B, Zhu Y. Microwave hydrothermal synthesis of $Bi_2Fe_4O_9$ crystals with visible light photocatalytic activity. Materials Chemistry and Physics. 2012;135(2):474–478.

[16] Tang P, Tong Y, Chen H, Cao F, Pan G. Microwave-assisted synthesis of nanoparticulate perovskite $LaFeO_3$ as a high active visible-light photocatalyst. Current Applied Physics. 2013;13(2):340–343.

[17] Sun Y, Wang W, Zhang L, Sun S, Gao E. Magnetic $ZnFe_2O_4$ octahedra: Synthesis and visible light induced photocatalytic activities. Materials Letters. 2013;98:124–127.

[18] Sun S, Yang X, Zhang Y, Zhang F, Ding J, Bao J, et al. Enhanced photocatalytic activity of sponge-like $ZnFe_2O_4$ synthesized by solution combustion method. Progress in Natural Science: Materials International. 2012;22(6):639–643.

[19] Xing J, Yang C, Li WK, Gong XQ, Yang HG. Soft chemistry synthesis of high-crystalline orthogermanate $CeGeO_4$: A new photocatalyst. Journal of Solid State Chemistry. 2013;197:204–208.

[20] Sun M, Li D, Zhang W, Chen Z, Huang H, Li W, et al. Rapid microwave hydrothermal synthesis of $ZnGa_2O_4$ with high photocatalytic activity toward aromatic compounds in air and dyes in liquid water. Journal of Solid State Chemistry. 2012;190:135–142.

[21] Guan M, Xiao C, Zhang J, Fan S, An R, Cheng Q, et al. Vacancy associates promoting solar-driven photocatalytic activity of ultrathin bismuth oxychloride nanosheets. Journal of the American Chemical Society. 2013;135(28):10411–10417.

[22] Li G, Qin F, Wang R, Xiao S, Sun H, Chen R. BiOX (X = Cl, Br, I) nanostructures: Mannitol-mediated microwave synthesis, visible light photocatalytic performance, and Cr(VI) removal capacity. Journal of Colloid and Interface Science. 2013;409:43–51.

[23] Qin X, Cheng H, Wang W, Huang B, Zhang X, Dai Y. Three dimensional BiOX (X = Cl, Br and I) hierarchical architectures: Facile ionic liquid-assisted solvothermal synthesis and photocatalysis towards organic dye degradation. Materials Letters. 2013;100:285–288.

[24] Zhang W, Zhang Q, Dong F. Visible-light photocatalytic removal of NO in air over BiOX (X = Cl, Br, I) single-crystal nanoplates prepared at room temperature. Industrial & Engineering Chemistry Research. 2013;52(20):6740–6746.

[25] Chen L, Yin S-F, Huang R, Zhou Y, Luo S-L, Au C-T. Facile synthesis of BiOCl nanoflowers of narrow band gap and their visible-light-induced photocatalytic property. Catalysis Communications. 2012;23:54–57.

[26] Ahern JC, Fairchild R, Thomas JS, Carr J, Patterson HH. Characterization of BiOX compounds as photocatalysts for the degradation of pharmaceuticals in water. Applied Catalysis B: Environmental. 2015;179:229–238.

[27] Zhang X, Wang X-B, Wang L-W, Wang W-K, Long LL, Li W-W, et al. Synthesis of a highly efficient BiOCl single-crystal nanodisk photocatalyst with exposing {001} facets. ACS Applied Materials & Interfaces. 2014;6(10):7766–7772.

[28] Cheng H, Huang B, Dai Y. Engineering BiOX (X = Cl, Br, I) nanostructures for highly efficient photocatalytic applications. Nanoscale. 2014;6(4):2009–2026.

[29] Pare B, Sarwan B, Jonnalagadda S. The characteristics and photocatalytic activities of BiOCl as highly efficient photocatalyst. Journal of Molecular Structure. 2012;1007:196–202.

[30] Huo Y, Zhang J, Miao M, Jin Y. Solvothermal synthesis of flower-like BiOBr microspheres with highly visible-light photocatalytic performances. Applied Catalysis B: Environmental. 2012;111:334–341.

[31] Liu Z, Wu B, Xiang D, Zhu Y. Effect of solvents on morphology and photocatalytic activity of BiOBr synthesized by solvothermal method. Materials Research Bulletin. 2012;47(11):3753–3757.

[32] Cao J, Zhou C, Lin H, Xu B, Chen S. Direct hydrolysis preparation of plate-like BiOI and their visible light photocatalytic activity for contaminant removal. Materials Letters. 2013;109:74–77.

[33] Shi X, Chen X, Chen X, Zhou S, Lou S. Solvothermal synthesis of BiOI hierarchical spheres with homogeneous sizes and their high photocatalytic performance. Materials Letters. 2012;68:296–299.

[34] Hao R, Xiao X, Zuo X, Nan J, Zhang W. Efficient adsorption and visible-light photocatalytic degradation of tetracycline hydrochloride using mesoporous BiOI microspheres. Journal of hazardous materials. 2012;209:137–145.

[35] Xiao X, Hao R, Zuo X, Nan J, Li L, Zhang W. Microwave-assisted synthesis of hierarchical $Bi_7O_9I_3$ microsheets for efficient photocatalytic degradation of bisphenol-A under visible light irradiation. Chemical Engineering Journal. 2012;209:293–300.

[36] Cao J, Li X, Lin H, Xu B, Luo B, Chen S. Low temperature synthesis of novel rodlike Bi_5O_7I with visible light photocatalytic performance. Materials Letters. 2012;76:181–183.

[37] Tang J, Li D, Feng Z, Long C. HgI_2: A novel photocatalyst with high performance in degradation of rhodamine B dyes under visible-light irradiation. Journal of Alloys and Compounds. 2015;653:310–314.

[38] Dai K, Lu L, Liu Z, Liu Q, Chen Z. A scalable synthesis technique of novel AgBr microcrystal and its visible light photocatalytic performance. Materials Letters. 2012;87:94–96.

[39] Liu L, Xu H, Li H, Xu Y, Xia J, Yin S. Synthesis and characterization of the efficient visible-light-induced photocatalyst AgBr and its photodegradation activity. Journal of Physics and Chemistry of Solids. 2012;73(4):523–529.

[40] Sun Y, Wang W, Zhang L, Sun S. The photocatalysis of Bi_2MoO_6 under the irradiation of blue LED. Materials Research Bulletin. 2013;48(10):4357–4361.

[41] Bi J, Che J, Wu L, Liu M. Effects of the solvent on the structure, morphology and photocatalytic properties of Bi_2MoO_6 in the solvothermal process. Materials Research Bulletin. 2013;48(6):2071–2075.

[42] Zhang Z, Wang W, Ren J, Xu J. Highly efficient photocatalyst Bi_2MoO_6 induced by blue light-emitting diode. Applied Catalysis B: Environmental. 2012;123:89–93.

[43] Zhang M, Shao C, Zhang P, Su C, Zhang X, Liang P, et al. Bi_2MoO_6 microtubes: Controlled fabrication by using electrospun polyacrylonitrile microfibers as template and their enhanced visible light photocatalytic activity. Journal of Hazardous Materials. 2012;225:155–163.

[44] Hernández-Uresti D, Martínez-de la Cruz A, Aguilar-Garib J. Photocatalytic activity of $PbMoO_4$ molybdate synthesized by microwave method. Catalysis Today. 2013;212:70–74.

[45] Hashim M, Hu C, Wang X, Li X, Guo D. Synthesis and photocatalytic property of lead molybdate dendrites with exposed (001) facet. Applied Surface Science. 2012;258(15): 5858–5862.

[46] Luévano-Hipólito E, Martínez-de la Cruz A, Yu Q, Brouwers H. Photocatalytic removal of nitric oxide by $Bi_2Mo_3O_{12}$ prepared by co-precipitation method. Applied Catalysis A: General. 2013;468:322–326.

[47] Wu W, Liang S, Chen Y, Shen L, Yuan R, Wu L. Mechanism and improvement of the visible light photocatalysis of organic pollutants over microcrystalline $AgNbO_3$ prepared by a sol–gel method. Materials Research Bulletin. 2013;48(4):1618–1626.

[48] Ai Z, Ho W, Lee S. A stable single-crystal Bi_3NbO_7 nanoplates superstructure for effective visible-light-driven photocatalytic removal of nitric oxide. Applied Surface Science. 2012;263:266–272.

[49] Liang S, Liang R, Wen L, Yuan R, Wu L, Fu X. Molecular recognitive photocatalytic degradation of various cationic pollutants by the selective adsorption on visible light-driven $SnNb_2O_6$ nanosheet photocatalyst. Applied Catalysis B: Environmental. 2012;125:103–110.

[50] Ameen S, Akhtar MS, Nazim M, Shin H-S. Rapid photocatalytic degradation of crystal violet dye over ZnO flower nanomaterials. Materials Letters. 2013;96:228–232.

[51] Mahmodi G, Sharifnia S, Madani M, Vatanpour V. Photoreduction of carbon dioxide in the presence of H_2, H_2O and CH_4 over TiO_2 and ZnO photocatalysts. Solar Energy. 2013;97:186–194.

[52] Li G, Liu Y. Photocatalytic degradation of methyl orange and gas-sensing performance of nanosized ZnO. Materials Science in Semiconductor Processing. 2013;16(3):792–796.

[53] Kansal SK, Lamba R, Mehta S, Umar A. Photocatalytic degradation of Alizarin Red S using simply synthesized ZnO nanoparticles. Materials Letters. 2013;106:385–389.

[54] Kumar R, Kumar G, Umar A. ZnO nano-mushrooms for photocatalytic degradation of methyl orange. Materials Letters. 2013;97:100–103.

[55] Lv Y, Pan C, Ma X, Zong R, Bai X, Zhu Y. Production of visible activity and UV performance enhancement of ZnO photocatalyst via vacuum deoxidation. Applied Catalysis B: Environmental. 2013;138:26–32.

[56] Muthirulan P, Meenakshisundararam M, Kannan N. Beneficial role of ZnO photocatalyst supported with porous activated carbon for the mineralization of alizarin cyanin green dye in aqueous solution. Journal of Advanced Research. 2013;4(6):479–484.

[57] Pei Z, Ding L, Hu J, Weng S, Zheng Z, Huang M, et al. Defect and its dominance in ZnO films: A new insight into the role of defect over photocatalytic activity. Applied Catalysis B: Environmental. 2013;142:736–743.

[58] Rahman QI, Ahmad M, Misra SK, Lohani MB. Hexagonal ZnO nanorods assembled flowers for photocatalytic dye degradation: Growth, structural and optical properties. Superlattices and Microstructures. 2013;64:495–506.

[59] Vu TT, del Río L, Valdés-Solís T, Marbán G. Fabrication of wire mesh-supported ZnO photocatalysts protected against photocorrosion. Applied Catalysis B: Environmental. 2013;140:189–198.

[60] Li J, Lu G, Wang Y, Guo Y, Guo Y. A high activity photocatalyst of hierarchical 3D flowerlike ZnO microspheres: Synthesis, characterization and catalytic activity. Journal of Colloid and Interface Science. 2012;377(1):191–196.

[61] Liu Y, Lv H, Li S, Xing X, Xi G. Preparation and photocatalytic property of hexagonal cylinder-like bipods ZnO microcrystal photocatalyst. Dyes and Pigments. 2012;95(3): 443–449.

[62] Xu F, Chen J, Guo L, Lei S, Ni Y. In situ electrochemically etching-derived ZnO nanotube arrays for highly efficient and facilely recyclable photocatalyst. Applied Surface Science. 2012;258(20):8160–8165.

[63] Khayyat SA, Akhtar M, Umar A. ZnO nanocapsules for photocatalytic degradation of thionine. Materials Letters. 2012;81:239–241.

[64] Jongnavakit P, Amornpitoksuk P, Suwanboon S, Ratana T. Surface and photocatalytic properties of ZnO thin film prepared by sol–gel method. Thin Solid Films. 2012;520(17): 5561–5567.

[65] Wang H, Dong S, Chang Y, Zhou X, Hu X. Microstructures and photocatalytic properties of porous ZnO films synthesized by chemical bath deposition method. Applied Surface Science. 2012;258(10):4288–4293.

[66] Hafez HS. Highly active ZnO rod-like nanomaterials: Synthesis, characterization and photocatalytic activity for dye removal. Physica E: Low-dimensional Systems and Nanostructures. 2012;44(7):1522–1527.

[67] Lee SD, Nam S-H, Kim M-H, Boo J-H. Synthesis and photocatalytic property of ZnO nanoparticles prepared by spray-pyrolysis method. Physics Procedia. 2012;32:320–326.

[68] Umar A, Akhtar M, Al-Hajry A, Al-Assiri M, Almehbad NY. Hydrothermally grown ZnO nanoflowers for environmental remediation and clean energy applications. Materials Research Bulletin. 2012;47(9):2407–2414.

[69] Anas S, Rahul S, Babitha K, Mangalaraja R, Ananthakumar S. Microwave accelerated synthesis of zinc oxide nanoplates and their enhanced photocatalytic activity under UV and solar illuminations. Applied Surface Science. 2015;355:98–103.

[70] Li Z, Zhang P, Shao T, Li X. In_2O_3 nanoporous nanosphere: A highly efficient photocatalyst for decomposition of perfluorooctanoic acid. Applied Catalysis B: Environmental. 2012;125:350–357.

[71] Bansal P, Chaudhary GR, Mehta S. Comparative study of catalytic activity of ZrO_2 nanoparticles for sonocatalytic and photocatalytic degradation of cationic and anionic dyes. Chemical Engineering Journal. 2015;280:475–485.

[72] Gao X, Su X, Yang C, Xiao F, Wang J, Cao X, et al. Hydrothermal synthesis of WO_3 nanoplates as highly sensitive cyclohexene sensor and high-efficiency MB photocatalyst. Sensors and Actuators B: Chemical. 2013;181:537–543.

[73] Huang J, Xiao L, Yang X. WO_3 nanoplates, hierarchical flower-like assemblies and their photocatalytic properties. Materials Research Bulletin. 2013;48(8):2782–2785.

[74] Ou JZ, Rani RA, Balendhran S, Zoolfakar AS, Field MR, Zhuiykov S, et al. Anodic formation of a thick three-dimensional nanoporous WO_3 film and its photocatalytic property. Electrochemistry Communications. 2013;27:128–132.

[75] Yamazaki S, Yamate T, Adachi K. Photocatalytic activity of aqueous WO_3 sol for the degradation of Orange II and 4-chlorophenol. Applied Catalysis A: General. 2013;454:30–36.

[76] Szilágyi IM, Fórizs B, Rosseler O, Szegedi Á, Németh P, Király P, et al. WO_3 photocatalysts: Influence of structure and composition. Journal of Catalysis. 2012;294:119–127.

[77] Kumar SG, Rao KK. Tungsten-based nanomaterials (WO_3 & Bi_2WO_6): Modifications related to charge carrier transfer mechanisms and photocatalytic applications. Applied Surface Science. 2015;355:939–958.

[78] Zhang G-Y, Feng Y, Xu Y-Y, Gao D-Z, Sun Y-Q. Controlled synthesis of mesoporous α-Fe_2O_3 nanorods and visible light photocatalytic property. Materials Research Bulletin. 2012;47(3):625–630.

[79] Iyyapushpam S, Nishanthi S, Padiyan DP. Photocatalytic degradation of methyl orange using α-Bi_2O_3 prepared without surfactant. Journal of Alloys and Compounds. 2013;563:104–107.

[80] Iyyapushpam S, Nishanthi S, Padiyan DP. Synthesis of room temperature bismuth oxide and its photocatalytic activity. Materials Letters. 2012;86:25–27.

[81] Riente P, Matas Adams A, Albero J, Palomares E, Pericàs MA. Light-driven organocatalysis using inexpensive, nontoxic Bi_2O_3 as the photocatalyst. Angewandte Chemie. 2014;126(36):9767–9770.

[82] Qin F, Zhao H, Li G, Yang H, Li J, Wang R, et al. Size-tunable fabrication of multifunctional Bi_2O_3 porous nanospheres for photocatalysis, bacteria inactivation and template-synthesis. Nanoscale. 2014;6(10):5402–5409.

[83] Qian J, Chen F, Wang F, Zhao X, Chen Z. Daylight photocatalysis performance of biomorphic CeO_2 hollow fibers prepared with lens cleaning paper as biotemplate. Materials Research Bulletin. 2012;47(8):1845–1848.

[84] Feng T, Wang X, Feng G. Synthesis of novel CeO_2 microspheres with enhanced solar light photocatalyic properties. Materials Letters. 2013;100:36–39.

[85] Ansari SA, Khan MM, Ansari MO, Kalathil S, Lee J, Cho MH. Band gap engineering of CeO_2 nanostructure using an electrochemically active biofilm for visible light applications. RSC Advances. 2014;4(32):16782–16791.

[86] Liyanage AD, Perera SD, Tan K, Chabal Y, Balkus KJ, Jr. Synthesis, characterization, and photocatalytic activity of Y-Doped CeO2 nanorods. ACS Catalysis. 2014;4(2):577–584.

[87] Li L, Zhang W, Feng C, Luan X, Jiang J, Zhang M. Preparation of nanocrystalline Cu_2O by a modified solid-state reaction method and its photocatalytic activity. Materials Letters. 2013;107:123–125.

[88] Li X, Zhen X, Meng S, Xian J, Shao Y, Fu X, et al. Structuring β-Ga_2O_3 photonic crystal photocatalyst for efficient degradation of organic pollutants. Environmental Science & Technology. 2013;47(17):9911–9917.

[89] Lopes OF, Paris EC, Ribeiro C. Synthesis of Nb_2O_5 nanoparticles through the oxidant peroxide method applied to organic pollutant photodegradation: A mechanistic study. Applied Catalysis B: Environmental. 2014;144:800–808.

[90] Katsumata H, Taniguchi M, Kaneco S, Suzuki T. Photocatalytic degradation of bisphenol A by Ag_3PO_4 under visible light. Catalysis Communications. 2013;34:30–34.

[91] Vu TA, Dao CD, Hoang TT, Nguyen KT, Le GH, Dang PT, et al. Highly photocatalytic activity of novel nano-sized Ag_3PO_4 for rhodamine B degradation under visible light irradiation. Materials Letters. 2013;92:57–60.

[92] Wan J, Sun L, Fan J, Liu E, Hu X, Tang C, et al. Facile synthesis of porous Ag_3PO_4 nanotubes for enhanced photocatalytic activity under visible light. Applied Surface Science. 2015;355:615–622.

[93] Pan C, Xu J, Chen Y, Zhu Y. Influence of OH-related defects on the performances of $BiPO_4$ photocatalyst for the degradation of rhodamine B. Applied Catalysis B: Environmental. 2012;115:314–319.

[94] Long B, Huang J, Wang X. Photocatalytic degradation of benzene in gas phase by nanostructured $BiPO_4$ catalysts. Progress in Natural Science: Materials International. 2012;22(6):644–653.

[95] Wang X, Li L, Lin Y, Zhu J. EDTA-assisted template-free synthesis and improved photocatalytic activity of homogeneous ZnSe hollow microspheres. Ceramics International. 2013;39(5):5213–5218.

[96] Chen Y, Li D, Chen J, Wang J, Meng S, Xian J, et al. A promising new photocatalyst $CdSnO_3 \cdot 3H_2O$ for air purification under ambient condition. Applied Catalysis B: Environmental. 2013;129:403–408.

[97] Foletto EL, Battiston S, Simões JM, Bassaco MM, Pereira LSF, de Moraes FloresÉM, et al. Synthesis of $ZnAl_2O_4$ nanoparticles by different routes and the effect of its pore size on the photocatalytic process. Microporous and Mesoporous Materials. 2012;163:29–33.

[98] Borhade AV, Baste YR. Study of photocatalytic asset of the $ZnSnO_3$ synthesized by green chemistry. Arabian Journal of Chemistry. 2012.

[99] Eskandari P, Kazemi F, Azizian-Kalandaragh Y. Convenient preparation of CdS nanostructures as a highly efficient photocatalyst under blue LED and solar light irradiation. Separation and Purification Technology. 2013;120:180–185.

[100] Chen F, Cao Y, Jia D, Niu X. Facile synthesis of CdS nanoparticles photocatalyst with high performance. Ceramics International. 2013;39(2):1511–1517.

[101] Li X, Xi Y, Hu C, Wang X. Water induced size and structure phase transition of CdS crystals and their photocatalytic property. Materials Research Bulletin. 2013;48(2):295–299.

[102] Deng C, Tian X. Facile microwave-assisted aqueous synthesis of CdS nanocrystals with their photocatalytic activities under visible lighting. Materials Research Bulletin. 2013;48(10):4344–4350.

[103] Patel JD, Mighri F, Ajji A, Chaudhuri TK. Fatty acid-assisted synthesis of CdS microspheres: Physicochemical properties and photocatalytic activity. Materials Letters. 2013;110:94–97.

[104] Chen F, Jia D, Cao Y, Jin X, Liu A. Facile synthesis of CdS nanorods with enhanced photocatalytic activity. Ceramics International. 2015;41(10):14604–14609.

[105] Chen F, Cao Y, Jia D. A facile route for the synthesis of ZnS rods with excellent photocatalytic activity. Chemical Engineering Journal. 2013;234:223–231.

[106] Dong F, Guo Y, Zhang J, Li Y, Yang L, Fang Q, et al. Size-controllable hydrothermal synthesis of ZnS nanospheres and the application in photocatalytic degradation of organic dyes. Materials Letters. 2013;97:59–63.

[107] Emin S, Lisjak D, Pitcher M, Valant M. Structural and morphological transformations of textural porous zinc sulfide microspheres. Microporous and Mesoporous Materials. 2013;165:185–192.

[108] Pal B, Pal B. Tuning the optical and photocatalytic properties of anisotropic ZnS nanostructures for the selective reduction of nitroaromatics. Chemical Engineering Journal. 2015;263:200–208.

[109] Liu H, Su Y, Chen P, Wang Y. Microwave-assisted solvothermal synthesis of 3D carnation-like SnS_2 nanostructures with high visible light photocatalytic activity. Journal of Molecular Catalysis A: Chemical. 2013;378:285–292.

[110] Umar A, Akhtar M, Dar G, Abaker M, Al-Hajry A, Baskoutas S. Visible-light-driven photocatalytic and chemical sensing properties of SnS_2 nanoflakes. Talanta. 2013;114:183–190.

[111] Park S, Park J, Selvaraj R, Kim Y. Facile microwave-assisted synthesis of SnS_2 nanoparticles for visible-light responsive photocatalyst. Journal of Industrial and Engineering Chemistry. 2015;31:269–275.

[112] Ferancova A, Rengaraj S, Kim Y, Vijayalakshmi S, Labuda J, Bobacka J, et al. Electrochemical study of novel nanostructured In_2S_3 and its effect on oxidative damage to DNA purine bases. Electrochimica Acta. 2013;92:124–131.

[113] Wu W, Lin R, Shen L, Liang R, Yuan R, Wu L. Visible-light-induced photocatalytic hydrogenation of 4-nitroaniline over In_2S_3 photocatalyst in water. Catalysis Communications. 2013;40:1–4.

[114] Biacchi AJ, Vaughn DD, Schaak RE. Synthesis and crystallographic analysis of shape-controlled SnS nanocrystal photocatalysts: Evidence for a pseudotetragonal structural modification. Journal of the American Chemical Society. 2013;135(31):11634–11644.

[115] Chen F, Cao Y, Jia D. Facile synthesis of Bi_2S_3 hierarchical nanostructure with enhanced photocatalytic activity. Journal of Colloid and Interface Science. 2013;404:110–116.

[116] Luo Y, Chen H, Li X, Gong Z, Wang X, Peng X, et al. Wet chemical synthesis of Bi_2S_3 nanorods for efficient photocatalysis. Materials Letters. 2013;105:12–15.

[117] Chen S, Zhang H, Fu X, Hu Y. Preparation, characterization, and photocatalytic performance of Ce_2S_3 for nitrobenzene reduction. Applied Surface Science. 2013;275:335–341.

[118] Chen Z, Xu J, Ren Z, He Y, Xiao G. Low temperature synthesis of $ZnIn_2S_4$ microspheres as a visible light photocatalyst for selective oxidation. Catalysis Communications. 2013;41:83–86.

[119] Wang W, Ng TW, Ho WK, Huang J, Liang S, An T, et al. $CdIn_2S_4$ microsphere as an efficient visible-light-driven photocatalyst for bacterial inactivation: Synthesis, characterizations and photocatalytic inactivation mechanisms. Applied Catalysis B: Environmental. 2013;129:482–490.

[120] Chen Z, Li D, Xiao G, He Y, Xu Y-J. Microwave-assisted hydrothermal synthesis of marigold-like $ZnIn_2$ S 4 microspheres and their visible light photocatalytic activity. Journal of Solid State Chemistry. 2012;186:247–254.

[121] Mu J, Wei Q, Yao P, Zhao X, Kang S-Z, Li X. Facile preparation and visible light photocatalytic activity of $CdIn_2S_4$ monodispersed spherical particles. Journal of Alloys and Compounds. 2012;513:506–509.

[122] Liang S, Lin Q, Zhu S, Wu L. PVP-assisted synthesis of porous strontium tantalate hydrate nanosphere and enhanced photocatalytic properties. Materials Letters. 2013;113:138–141.

[123] Maia D, Pepe I, da Silva AF, Silva L. Visible-light-driven photocatalytic hydrogen production over dye-sensitized β-$BiTaO_4$. Journal of Photochemistry and Photobiology A: Chemistry. 2012;243:61–64.

[124] Androš L, Jurić M, Popović J, Šantić A, Lazić P, Benčina M, et al. $Ba_4Ta_2O_9$ Oxide prepared from an oxalate-based molecular precursor—characterization and properties. Inorganic Chemistry. 2013;52(24):14299–14308.

[125] Siddiqui MA, Chandel VS, Azam A. Comparative study of potassium hexatitanate ($K_2Ti_6O_{13}$) whiskers prepared by sol–gel and solid state reaction routes. Applied Surface Science. 2012;258(19):7354–7358.

[126] Zhang X, Li T, Gong Z, Zhao H, Wang L, Wan J, et al. Shape controlled $FeTiO_3$ nanostructures: Crystal facet and photocatalytic property. Journal of Alloys and Compounds. 2015;653:619–623.

[127] Cui Y, Briscoe J, Dunn S. Effect of ferroelectricity on solar-light-driven photocatalytic activity of $BaTiO_3$ influence on the carrier separation and Stern layer formation. Chemistry of Materials. 2013;25(21):4215–4223.

[128] Dumrongrojthanath P, Thongtem T, Phuruangrat A, Thongtem S. Hydrothermal synthesis of Bi_2WO_6 hierarchical flowers with their photonic and photocatalytic properties. Superlattices and Microstructures. 2013;54:71–77.

[129] Saison T, Gras P, Chemin N, Chanéac C, Durupthy O, Brezova V, et al. New insights into Bi_2WO_6 properties as a visible-light photocatalyst. The Journal of Physical Chemistry C. 2013;117(44):22656–22666.

[130] Pei CC, Chu W. The photocatalyic degradation and modeling of 2,4-dichlorophenoxyacetic acid by bismuth tungstate/peroxide. Chemical Engineering Journal. 2013;223:665–669.

[131] Duan F, Zhang Q, Shi D, Chen M. Enhanced visible light photocatalytic activity of Bi_2WO_6 via modification with polypyrrole. Applied Surface Science. 2013;268:129–135.

[132] Liu Y, Li Z, Lv H, Tang H, Xing X. Synthesis of hierarchical Bi_2WO_6 microspheres with high visible-light-driven photocatalytic activities by sol–gel-hydrothermal route. Materials Letters. 2013;108:84–87.

[133] Hu S-P, Xu C-Y, Zhen L. Solvothermal synthesis of Bi_2WO_6 hollow structures with excellent visible-light photocatalytic properties. Materials Letters. 2013;95:117–120.

[134] Yan Y, Wu Y, Yan Y, Guan W, Shi W. Inorganic-salt-assisted morphological evolution and visible-light-driven photocatalytic performance of Bi_2WO_6 nanostructures. The Journal of Physical Chemistry C. 2013;117(39):20017–20028.

[135] Zhang F-J, Xie F-Z, Liu J, Zhao W, Zhang K. Rapid sonochemical synthesis of irregular nanolaminar-like Bi_2WO_6 as efficient visible-light-active photocatalysts. Ultrasonics Sonochemistry. 2013;20(1):209–215.

[136] Zhao G, Liu S, Lu Q, Xu F, Sun H. Fabrication of electrospun Bi_2WO_6 microbelts with enhanced visible photocatalytic degradation activity. Journal of Alloys and Compounds. 2013;578:12–16.

[137] Zhuo Y, Huang J, Cao L, Ouyang H, Wu J. Photocatalytic activity of snow-like Bi_2WO_6 microcrystalline for decomposition of rhodamine B under natural sunlight irradiation. Materials Letters. 2013;90:107–110.

[138] Huang H, Chen H, Xia Y, Tao X, Gan Y, Weng X, et al. Controllable synthesis and visible-light-responsive photocatalytic activity of Bi_2WO_6 fluffy microsphere with hierarchical architecture. Journal of Colloid and Interface Science. 2012;370(1):132–138.

[139] He J, Wang W, Long F, Zou Z, Fu Z, Xu Z. Hydrothermal synthesis of hierarchical rose-like Bi_2WO_6 microspheres with high photocatalytic activities under visible-light irradiation. Materials Science and Engineering: B. 2012;177(12):967–974.

[140] Guo J, Zhou X, Lu Y, Zhang X, Kuang S, Hou W. Monodisperse spindle-like $FeWO_4$ nanoparticles: Controlled hydrothermal synthesis and enhanced optical properties. Journal of Solid State Chemistry. 2012;196:550–556.

[141] Cavalcante L, Sczancoski J, Batista N, Longo E, Varela JA, Orlandi M. Growth mechanism and photocatalytic properties of $SrWO_4$ microcrystals synthesized by injection of ions into a hot aqueous solution. Advanced Powder Technology. 2013;24(1):344–353.

[142] Molinari A, Argazzi R, Maldotti A. Photocatalysis with $Na_4W_{10}O_{32}$ in water system: Formation and reactivity of OH radicals. Journal of Molecular Catalysis A: Chemical. 2013;372:23–28.

[143] Karthiga R, Kavitha B, Rajarajan M, Suganthi A. Photocatalytic and antimicrobial activity of $NiWO_4$ nanoparticles stabilized by the plant extract. Materials Science in Semiconductor Processing. 2015;40:123–129.

[144] Yu C, Cao F, Li X, Li G, Xie Y, Jimmy CY, et al. Hydrothermal synthesis and characterization of novel $PbWO_4$ microspheres with hierarchical nanostructures and enhanced photocatalytic performance in dye degradation. Chemical Engineering Journal. 2013;219:86–95.

[145] Lin X, Li H, Yu L, Zhao H, Yan Y, Liu C, et al. Efficient removal rhodamine B over hydrothermally synthesized fishbone like $BiVO_4$. Materials Research Bulletin. 2013;48(10):4424–4429.

[146] Obregón S, Colón G. On the different photocatalytic performance of $BiVO_4$ catalysts for methylene blue and rhodamine B degradation. Journal of Molecular Catalysis A: Chemical. 2013;376:40–47.

[147] Sun J, Chen G, Wu J, Dong H, Xiong G. Bismuth vanadate hollow spheres: Bubble template synthesis and enhanced photocatalytic properties for photodegradation. Applied Catalysis B: Environmental. 2013;132:304–314.

[148] Tan G, Zhang L, Ren H, Wei S, Huang J, Xia A. Effects of pH on the hierarchical structures and photocatalytic performance of $BiVO_4$ powders prepared via the microwave hydrothermal method. ACS Applied Materials & Interfaces. 2013;5(11):5186–5193.

[149] Yao M, Liu M, Gan L, Zhao F, Fan X, Zhu D, et al. Monoclinic mesoporous $BiVO_4$: Synthesis and visible-light-driven photocatalytic property. Colloids and Surfaces A: Physicochemical and Engineering Aspects. 2013;433:132–138.

[150] Zhang Y, Li G, Yang X, Yang H, Lu Z, Chen R. Monoclinic $BiVO_4$ micro-/nanostructures: Microwave and ultrasonic wave combined synthesis and their visible-light photocatalytic activities. Journal of Alloys and Compounds. 2013;551:544–550.

[151] Lei B-X, Zhang P, Wang S-N, Li Y, Huang G-L, Sun Z-F. Additive-free hydrothermal synthesis of novel bismuth vanadium oxide dendritic structures as highly efficient visible-light photocatalysts. Materials Science in Semiconductor Processing. 2015;30:429–434.

[152] Wang X, Li G, Ding J, Peng H, Chen K. Facile synthesis and photocatalytic activity of monoclinic $BiVO_4$ micro/nanostructures with controllable morphologies. Materials Research Bulletin. 2012;47(11):3814–3818.

[153] Shi W, Yan Y, Yan X. Microwave-assisted synthesis of nano-scale $BiVO_4$ photocatalysts and their excellent visible-light-driven photocatalytic activity for the degradation of ciprofloxacin. Chemical Engineering Journal. 2013;215:740–746.

[154] Zhang J, Cui H, Wang B, Li C, Zhai J, Li Q. Fly ash cenospheres supported visible-light-driven $BiVO_4$ photocatalyst: Synthesis, characterization and photocatalytic application. Chemical Engineering Journal. 2013;223:737–746.

[155] Ressnig D, Kontic R, Patzke GR. Morphology control of $BiVO_4$ photocatalysts: pH optimization vs. self-organization. Materials Chemistry and Physics. 2012;135(2):457–466.

[156] Jiang H, Meng X, Dai H, Deng J, Liu Y, Zhang L, et al. High-performance porous spherical or octapod-like single-crystalline $BiVO_4$ photocatalysts for the removal of phenol and methylene blue under visible-light illumination. Journal of Hazardous Materials. 2012;217:92–99.

[157] Abdullah AH, Moey HJM, Yusof NA. Response surface methodology analysis of the photocatalytic removal of Methylene Blue using bismuth vanadate prepared via polyol route. Journal of Environmental Sciences. 2012;24(9):1694–1701.

[158] Chen L, Wang J, Meng D, Xing Y, Tian X, Yu X, et al. Effects of citric acid and urea on the structural and morphological characteristics of $BiVO_4$ synthesized by the sol–gel combustion method. Journal of Sol-Gel Science and Technology. 2015;76(3):562–571.

[159] Ju P, Fan H, Zhang B, Shang K, Liu T, Ai S, et al. Enhanced photocatalytic activity of β-$AgVO_3$ nanowires loaded with Ag nanoparticles under visible light irradiation. Separation and Purification Technology. 2013;109:107–110.

[160] Belver C, Adán C, García-Rodríguez S, Fernández-García M. Photocatalytic behavior of silver vanadates: Microemulsion synthesis and post-reaction characterization. Chemical Engineering Journal. 2013;224:24–31.

[161] Wang Y, Dai H, Deng J, Liu Y, Zhao Z, Li X, et al. Three-dimensionally ordered macroporous $InVO_4$: fabrication and excellent visible-light-driven photocatalytic performance for methylene blue degradation. Chemical Engineering Journal. 2013;226:87–94.

[162] Yan Y, Liu X, Fan W, Lv P, Shi W. $InVO_4$ microspheres: Preparation, characterization and visible-light-driven photocatalytic activities. Chemical Engineering Journal. 2012;200:310–316.

[163] Noh TH, Kim DW, Seo SW, Cho IS, Kim DH, Han HS, et al. Facile hydrothermal synthesis of $InVO_4$ microspheres and their visible-light photocatalytic activities. Materials Letters. 2012;72:98–100.

[164] Ozturk B, Soylu GSP. Synthesis of surfactant-assisted $FeVO_4$ nanostructure: Characterization and photocatalytic degradation of phenol. Journal of Molecular Catalysis A: Chemical. 2015;398:65–71.

[165] Zhang S, Sun Y, Li C, Ci L. $Cu_3V_2O_8$ hollow spheres in photocatalysis and primary lithium batteries. Solid State Sciences. 2013;25:15–21.

[166] Zheng F, Zhang M, Guo M. Controllable preparation of WO_3 nanorod arrays by hydrothermal method. Thin Solid Films. 2013;534:45–53.

[167] Grabowska E. Selected perovskite oxides: Characterization, preparation and photocatalytic properties—A review. Applied Catalysis B: Environmental. 2016;186:97–126.

[168] Dahl M, Liu Y, Yin Y. Composite titanium dioxide nanomaterials. Chemical Reviews. 2014;114(19):9853–9889.

[169] Tian J, Zhao Z, Kumar A, Boughton RI, Liu H. Recent progress in design, synthesis, and applications of one-dimensional TiO_2 nanostructured surface heterostructures: A review. Chemical Society Reviews. 2014;43(20):6920–6937.

[170] J. McKone and N. Lewis, in Photoelectrochemical Water Splitting: Materials, Processes and Architectures, The Royal Society of Chemistry, 2013, pp. 52–82 Editor(s): Hans-Joachim Lewerenz, Laurie Peter.

[171] Martha S, Sahoo PC, Parida KM. An overview on visible light responsive metal oxide based photocatalysts for hydrogen energy production. Rsc Advances. 2015;5(76): 61535–61553.

[172] Zhang S, Chen Q, Wang Y, Guo L. Synthesis and photoactivity of CdS photocatalysts modified by polypyrrole. International Journal of Hydrogen Energy. 2012;37(17): 13030–13036.

[173] Ding J, Sun S, Yan W, Bao J, Gao C. Photocatalytic H-2 evolution on a novel $CaIn_2S_4$ photocatalyst under visible light irradiation. International Journal of Hydrogen Energy. 2013;38(30):13153–13158.

[174] Kim J, Sohn Y, Kang M. New fan blade-like core-shell $Sb_2Ti_xS_y$ photocatalytic nanorod for hydrogen production from methanol/water photolysis. International Journal of Hydrogen Energy. 2013;38(5):2136–2143.

[175] Zhang X, Yang M, Zhao J, Guo L. Photocatalytic hydrogen evolution with simultaneous degradation of organics over $(CuIn)_{(0.2)}Zn_{1.6}S_2$ solid solution. International Journal of Hydrogen Energy. 2013;38(36):15985–15991.

[176] Song K, Zhu R, Tian F, Cao G, Ouyang F. Effects of indium contents on photocatalytic performance of ZnIn2S4 for hydrogen evolution under visible light. Journal of Solid State Chemistry. 2015;232:138–143.

[177] Chen F, Zai J, Xu M, Qian X. 3D-hierarchical Cu_3SnS_4 flowerlike microspheres: Controlled synthesis, formation mechanism and photocatalytic activity for H-2 evolution from water. Journal of Materials Chemistry A. 2013;1(13):4316–4323.

[178] Liu M, Zhang L, He X, Zhang B, Song H, Li S, et al. L-Cystine-assisted hydrothermal synthesis of $Mn_{1-x}Cd_xS$ solid solutions with hexagonal wurtzite structure for efficient photocatalytic hydrogen evolution under visible light irradiation. Journal of Materials Chemistry A. 2014;2(13):4619–4626.

[179] Lin S, Shi L, Yoshida H, Li MR, Zou XD. Synthesis of hollow spherical tantalum oxide nanoparticles and their photocatalytic activity for hydrogen production. Journal of Solid State Chemistry. 2013;199:15–20.

[180] Liao LB, Zhang QH, Su ZH, Zhao ZZ, Wang YN, Li Y, et al. Efficient solar water-splitting using a nanocrystalline CoO photocatalyst. Nature Nanotechnology. 2014;9(1):69–73.

[181] GurudayalChiam SY, Kumar MH, Bassi PS, Seng HL, Barber J, et al. Improving the efficiency of hematite nanorods for photoelectrochemical water splitting by doping with manganese. Acs Applied Materials & Interfaces. 2014;6(8):5852–5859.

[182] Yan Y, Cai F, Song Y, Shi W. $InVO_4$ nanocrystal photocatalysts: Microwave-assisted synthesis and size-dependent activities of hydrogen production from water splitting under visible light. Chemical Engineering Journal. 2013;233:1–7.

[183] Li P, Umezawa N, Abe H, Ye J. Novel visible-light sensitive vanadate photocatalysts for water oxidation: Implications from density functional theory calculations. Journal of Materials Chemistry A. 2015;3(20):10720–10723.

[184] Xie Q, Wang Y, Pan B, Wang H, Su W, Wang X. A novel photocatalyst LaOF: Facile fabrication and photocatalytic hydrogen production. Catalysis Communications. 2012;27:21–25.

[185] Jiang W, Jiao XL, Chen DR. Photocatalytic water splitting of surfactant-free fabricated high surface area NaTaO3 nanocrystals. International Journal of Hydrogen Energy. 2013;38(29):12739–12746.

[186] Yang H, Liu X, Zhou Z, Guo L. Preparation of a novel $Cd_2Ta_2O_7$ photocatalyst and its photocatalytic activity in water splitting. Catalysis Communications. 2013;31:71–75.

[187] Dhanasekaran P, Gupta NM. Factors affecting the production of H_2 by water splitting over a novel visible-light-driven photocatalyst GaFeO3. International Journal of Hydrogen Energy. 2012;37(6):4897–4907.

[188] Tijare SN, Joshi MV, Padole PS, Mangrulkar PA, Rayalu SS, Labhsetwar NK. Photocatalytic hydrogen generation through water splitting on nano-crystalline $LaFeO_3$ perovskite. International Journal of Hydrogen Energy. 2012;37(13):10451–10456.

[189] Takimoto Y, Kitta T, Irie H. Visible-light sensitive hydrogen evolution photocatalyst ZnRh2O4. International Journal of Hydrogen Energy. 2012;37(1):134–138.

[190] Peng T, Zhang X, Lv H, Zan L. Preparation of $NiFe_2O_4$ nanoparticles and its visible-light-driven photoactivity for hydrogen production. Catalysis Communications. 2012;28:116–119.

[191] Wang Z, Wang JT, Hou JG, Huang K, Jiao SQ, Zhu HM. Facile synthesis of efficient photocatalytic tantalum nitride nanoparticles. Materials Research Bulletin. 2012;47(11): 3605–3611.

[192] Shen J, Zai J, Yuan Y, Qian X. 3D hierarchical ZnIn2S4: The preparation and photocatalytic properties on water splitting. International Journal of Hydrogen Energy. 2012;37(22):16986–16993.

[193] Wang L, Wang W. Photocatalytic hydrogen production from aqueous solutions over novel Bi0.5Na0.5TiO3 microspheres. International Journal of Hydrogen Energy. 2012;37(4):3041–3047.

[194] Li Q, Meng H, Zhou P, Zheng Y, Wang J, Yu J, et al. $Zn_{1-x}Cd_xS$ solid solutions with controlled bandgap and enhanced visible-light photocatalytic H-2-production activity. Acs Catalysis. 2013;3(5):882–889.

[195] Liu M, Jing D, Zhou Z, Guo L. Twin-induced one-dimensional homojunctions yield high quantum efficiency for solar hydrogen generation. Nature Communications. 2013;4.

[196] Chen W, Li C, Gao H, Yuan J, Shangguan W, Su J, et al. Photocatalytic water splitting on protonated form of layered perovskites $K_{0.5}La_{0.5}Bi_2M_2O_9$ (M = Ta; Nb) by ion-exchange. International Journal of Hydrogen Energy. 2012;37(17):12846–12851.

[197] Li X, Yu J, Low J, Fang Y, Xiao J, Chen X. Engineering heterogeneous semiconductors for solar water splitting. Journal of Materials Chemistry A. 2015;3(6):2485–2534.

[198] Zaleska A. Doped-TiO_2: A review. Recent Patents on Engineering. 2008;2(3):157–164.

[199] Ghugal SG, Umare SS, Sasikala R. A stable, efficient and reusable CdS–SnO_2 heterostructured photocatalyst for the mineralization of acid Violet 7 dye. Applied Catalysis A: General. 2015;496:25–31.

[200] Hamrouni A, Moussa N, Di Paola A, Palmisano L, Houas A, Parrino F. Photocatalytic activity of binary and ternary SnO_2–ZnO–$ZnWO_4$ nanocomposites. Journal of Photochemistry and Photobiology A: Chemistry. 2015;309:47–54.

[201] Balachandran S, Swaminathan M. Facile fabrication of heterostructured Bi_2O_3–ZnO photocatalyst and its enhanced photocatalytic activity. The Journal of Physical Chemistry C. 2012;116(50):26306–26312.

[202] Cheng L, Kang Y. Synthesis and characterization of Bi_2O_3/$NaBiO_3$ composite visible light-driven photocatalyst. Materials Letters. 2013;97:125–128.

[203] Cheng L, Kang Y. Synthesis of $NaBiO_3/Bi_2O_3$ heterojunction-structured photocatalyst and its photocatalytic mechanism. Materials Letters. 2014;117:94–97.

[204] Fan H, Li H, Liu B, Lu Y, Xie T, Wang D. Photoinduced charge transfer properties and photocatalytic activity in $Bi_2O_3/BaTiO_3$ composite photocatalyst. ACS Applied Materials & Interfaces. 2012;4(9):4853–4857.

[205] Liu J, Wei R, Hu J, Li L, Li J. Novel $Bi_2O_3/NaBi(MoO_4)_2$ heterojunction with enhanced photocatalytic activity under visible light irradiation. Journal of Alloys and Compounds. 2013;580:475–480.

[206] Cheng L, Liu X, Kang Y. Bi_5O_7I/Bi_2O_3: A novel heterojunction-structured visible light-driven photocatalyst. Materials Letters. 2014;134:218–221.

[207] Cheng L, Kang Y. Bi_5O_7I/Bi_2O_3 composite photocatalyst with enhanced visible light photocatalytic activity. Catalysis Communications. 2015;72:16–19.

[208] Li X, Huang R, Hu Y, Chen Y, Liu W, Yuan R, et al. A templated method to Bi_2WO_6 hollow microspheres and their conversion to double-shell Bi2O3/Bi2WO6 hollow microspheres with improved photocatalytic performance. Inorganic Chemistry. 2012;51(11):6245–6250.

[209] Hojamberdiev M, Katsumata K-I, Morita K, Bilmes SA, Matsushita N, Okada K. One-step hydrothermal synthesis and photocatalytic performance of $ZnWO_4/Bi_2WO_6$ composite photocatalysts for efficient degradation of acetaldehyde under UV light irradiation. Applied Catalysis A: General. 2013;457:12–20.

[210] Issarapanacheewin S, Wetchakun K, Phanichphant S, Kangwansupamonkon W, Wetchakun N. A novel CeO_2/Bi_2WO_6 composite with highly enhanced photocatalytic activity. Materials Letters. 2015;156:28–31.

[211] Zhang X, Zhang L, Hu J-S, Pan C-L, Hou C-M. Facile hydrothermal synthesis of novel $Bi_{12}TiO_{20}$-Bi_2WO_6 heterostructure photocatalyst with enhanced photocatalytic activity. Applied Surface Science. 2015;346:33–40.

[212] Feng Y, Yan X, Liu C, Hong Y, Zhu L, Zhou M, et al. Hydrothermal synthesis of CdS/Bi_2MoO_6 heterojunction photocatalysts with excellent visible-light-driven photocatalytic performance. Applied Surface Science. 2015;353:87–94.

[213] Xu J, Cao X. Characterization and mechanism of MoS_2/CdS composite photocatalyst used for hydrogen production from water splitting under visible light. Chemical Engineering Journal. 2015;260:642–648.

[214] Chen G, Li D, Li F, Fan Y, Zhao H, Luo Y, et al. Ball-milling combined calcination synthesis of MoS_2/CdS photocatalysts for high photocatalytic H 2 evolution activity under visible light irradiation. Applied Catalysis A: General. 2012;443:138–144.

[215] Duo F, Fan C, Wang Y, Cao Y, Zhang X. One-pot hydrothermal synthesis of a novel $BiPO_4$/BiOBr composite with enhanced visible light photocatalytic activities. Materials Science in Semiconductor Processing. 2015;38:157–164.

[216] Liu ZS, Wu BT, Niu JN, Feng PZ, Zhu YB. $BiPO_4$/BiOBr p–n junction photocatalysts: One-pot synthesis and dramatic visible light photocatalytic activity. Materials Research Bulletin. 2015;63:187–193.

[217] Duo F, Wang Y, Mao X, Zhang X, Wang Y, Fan C. A $BiPO_4$/BiOCl heterojunction photocatalyst with enhanced electron-hole separation and excellent photocatalytic performance. Applied Surface Science. 2015;340:35–42.

[218] Lin X, Liu D, Guo X, Sun N, Zhao S, Chang L, et al. Fabrication and efficient visible light-induced photocatalytic activity of Bi_2MoO_6/$BiPO_4$ composite. Journal of Physics and Chemistry of Solids. 2015;76:170–177.

[219] Huang H, Liu L, Zhang Y, Tian N. One pot hydrothermal synthesis of a novel $BiIO_4$/Bi_2MoO_6 heterojunction photocatalyst with enhanced visible-light-driven photocatalytic activity for rhodamine B degradation and photocurrent generation. Journal of Alloys and Compounds. 2015;619:807–811.

[220] Wang W, Huang X, Wu S, Zhou Y, Wang L, Shi H, et al. Preparation of p–n junction Cu_2O/$BiVO_4$ heterogeneous nanostructures with enhanced visible-light photocatalytic activity. Applied Catalysis B: Environmental. 2013;134:293–301.

[221] Min S, Wang F, Jin Z, Xu J. Cu_2 O nanoparticles decorated $BiVO_4$ as an effective visible-light-driven pn heterojunction photocatalyst for methylene blue degradation. Superlattices and Microstructures. 2014;74:294–307.

[222] Li J, Zhao W, Guo Y, Wei Z, Han M, He H, et al. Facile synthesis and high activity of novel $BiVO_4$/$FeVO_4$ heterojunction photocatalys for degradation of metronidazole. Applied Surface Science. 2015.

[223] Lv C, Chen G, Sun J, Zhou Y, Fan S, Zhang C. Realizing nanosized interfacial contact via constructing $BiVO_4$/$Bi_4V_2O_{11}$ element-copied heterojunction nanofibres for superior photocatalytic properties. Applied Catalysis B: Environmental. 2015;179:54–60.

[224] Mehraj O, Mir NA, Pirzada BM, Sabir S. Fabrication of novel Ag_3PO_4/BiOBr heterojunction with high stability and enhanced visible-light-driven photocatalytic activity. Applied Surface Science. 2015;332:419–429.

[225] Lin L, Huang M, Long L, Sun Z, Zheng W, Chen D. Fabrication of a three-dimensional BiOBr/BiOI photocatalyst with enhanced visible light photocatalytic performance. Ceramics International. 2014;40(8):11493–11501.

[226] Lin H, Ye H, Li X, Cao J, Chen S. Facile anion-exchange synthesis of BiOI/BiOBr composite with enhanced photoelectrochemical and photocatalytic properties. Ceramics International. 2014;40(7):9743–9750.

[227] Liu Z, Ran H, Wu B, Feng P, Zhu Y. Synthesis and characterization of BiOI/BiOBr heterostructure films with enhanced visible light photocatalytic activity. Colloids and Surfaces A: Physicochemical and Engineering Aspects. 2014;452:109–114.

[228] Luo J, Zhou X, Ma L, Xu X. Enhanced visible-light-driven photocatalytic activity of WO_3/BiOI heterojunction photocatalysts. Journal of Molecular Catalysis A: Chemical. 2015;410:168–176.

[229] Cao J, Luo B, Lin H, Xu B, Chen S. Thermodecomposition synthesis of WO_3/H_2WO_4 heterostructures with enhanced visible light photocatalytic properties. Applied Catalysis B: Environmental. 2012;111:288–296.

[230] Chen X, Dai Y, Huang W. Novel $Ag_3PO_4/ZnFe_2O_4$ composite photocatalyst with enhanced visible light photocatalytic activity. Materials Letters. 2015;145:125–128.

[231] Zhang L, He Y, Ye P, Qin W, Wu Y, Wu T. Enhanced photodegradation activity of Rhodamine B by Co_3O_4/Ag_3VO_4 under visible light irradiation. Materials Science and Engineering: B. 2013;178(1):45–52.

[232] Zhang L, He Y, Ye P, Wu Y, Wu T. Visible light photocatalytic activities of $ZnFe_2O_4$ loaded by Ag_3VO_4 heterojunction composites. Journal of Alloys and Compounds. 2013;549:105–113.

[233] Song L, Li Y, Tian H, Wu X, Fang S, Zhang S. Synthesis of $AgBr/Ag_4P_2O_7$ composite photocatalyst and enhanced photocatalytic performance. Materials Science and Engineering: B. 2014;189:70–75.

[234] Krishnakumar B, Subash B, Swaminathan M. AgBr–ZnO–An efficient nano-photocatalyst for the mineralization of acid Black 1 with UV light. Separation and Purification Technology. 2012;85:35–44.

[235] Pirhashemi M, Habibi-Yangjeh A. Simple and large scale one-pot method for preparation of AgBr–ZnO nanocomposites as highly efficient visible light photocatalyst. Applied Surface Science. 2013;283:1080–1088.

[236] Shi L, Liang L, Ma J, Sun J. Improved photocatalytic performance over AgBr/ZnO under visible light. Superlattices and Microstructures. 2013;62:128–139.

[237] Wu C, Shen L, Zhang YC, Huang Q. Synthesis of AgBr/ZnO nanocomposite with visible light-driven photocatalytic activity. Materials Letters. 2012;66(1):83–85.

[238] Subash B, Krishnakumar B, Pandiyan V, Swaminathan M, Shanthi M. An efficient nanostructured Ag_2S–ZnO for degradation of Acid Black 1 dye under day light illumination. Separation and Purification Technology. 2012;96:204–213.

[239] Shaker-Agjekandy S, Habibi-Yangjeh A. Facile one-pot method for preparation of AgI/ZnO nanocomposites as visible-light-driven photocatalysts with enhanced activities. Materials Science in Semiconductor Processing. 2015;34:74–81.

[240] Yu C, Wei L, Zhou W, Chen J, Fan Q, Liu H. Enhancement of the visible light activity and stability of Ag_2CO_3 by formation of AgI/Ag 2 CO 3 heterojunction. Applied Surface Science. 2014;319:312–318.

[241] Nashim A, Parida K. Novel $Sm_2Ti_2O_7/SmCrO_3$ heterojunction based composite photocatalyst for degradation of rhodamine 6G dye. Chemical Engineering Journal. 2013;215:608–615.

[242] Zhang F, Li X, Zhao Q, Zhang Q, Tadé M, Liu S. Fabrication of α-Fe_2O_3/In_2O_3 composite hollow microspheres: A novel hybrid photocatalyst for toluene degradation under visible light. Journal of Colloid and Interface Science. 2015;457:18–26.

[243] Serpone N, Emeline A. Semiconductor photocatalysis—past, present, and future outlook. The Journal of Physical Chemistry Letters. 2012;3(5):673–677.

[244] Bajorowicz B, Cybula A, Winiarski MJ, Klimczuk T, Zaleska A. Surface properties and photocatalytic activity of $KTaO_3$, CdS, MoS_2 semiconductors and their binary and ternary semiconductor composites. Molecules. 2014;19(9):15339–15360.

[245] Marchelek M, Bajorowicz B, Mazierski P, Cybula A, Klimczuk T, Winiarski M, et al. $KTaO_3$ based nanocomposites for air treatment., Catalysis Today 252 (2014) 47-53.

[246] Hong E, Kim D, Kim JH. Heterostructured metal sulfide (ZnS–CuS–CdS) photocatalyst for high electron utilization in hydrogen production from solar water splitting. Journal of Industrial and Engineering Chemistry. 2014;20(5):3869–3874.

[247] Pirhashemi M, Habibi-Yangjeh A. Ternary $ZnO/AgBr/Ag_2CrO_4$ nanocomposites with tandem n–n heterojunctions as novel visible-light-driven photocatalysts with excellent activity. Ceramics International. 2015;41(10):14383–14393.

[248] Chen X, Li L, Zhang W, Li Y, Song Q, Zhang J, et al. Multi-pathway photoelectron migration in globular flower-like $In_2O_3/AgBr/Bi_2WO_6$ synthesized by microwave-assisted method with enhanced photocatalytic activity. Journal of Molecular Catalysis A: Chemical. 2016;414:27–36.

[249] Shekofteh-Gohari M, Habibi-Yangjeh A. Ternary $ZnO/Ag_3VO_4/Fe_3O_4$ nanocomposites: Novel magnetically separable photocatalyst for efficiently degradation of dye pollutants under visible-light irradiation. Solid State Sciences. 2015;48:177–185.

[250] Shekofteh-Gohari M, Habibi-Yangjeh A. Ultrasonic-assisted preparation of novel ternary $ZnO/AgI/Fe_3O_4$ nanocomposites as magnetically separable visible-light-driven photocatalysts with excellent activity. Journal of colloid and interface science. 2016;461:144–153.

[251] Shaker-Agjekandy S, Habibi-Yangjeh A. Ultrasonic-assisted preparation of novel ternary $ZnO/AgI/Ag_2CrO_4$ nanocomposites as visible-light-driven photocatalysts with excellent activity. Materials Science in Semiconductor Processing. 2016;44:48–56.

[252] Liu C, Liu Z, Li Y, Liu Z, Wang Y, Lei E, et al. Enhanced visible-light-responsive photocatalytic property of CdS and PbS sensitized ZnO nanocomposite photocatalysts. Materials Science and Engineering: B. 2012;177(8):570–574.

[253] Shekofteh-Gohari M, Habibi-Yangjeh A. Facile preparation of Fe_3O_4@ AgBr–ZnO nanocomposites as novel magnetically separable visible-light-driven photocatalysts. Ceramics International. 2015;41(1):1467–1476.

[254] Hou X, Tian Y, Zhang X, Dou S, Pan L, Wang W, et al. Preparation and characterization of $Fe_3O_4/SiO_2/Bi_2MoO_6$ composite as magnetically separable photocatalyst. Journal of Alloys and Compounds. 2015;638:214–220.

[255] Zhang L, Wang W, Sun S, Sun Y, Gao E, Zhang Z. Elimination of BPA endocrine disruptor by magnetic BiOBr@ SiO_2@ Fe_3O_4 photocatalyst. Applied Catalysis B: Environmental. 2014;148:164–169.

[256] Huang Y, Fan W, Long B, Li H, Zhao F, Liu Z, et al. Visible light $Bi_2S_3/Bi_2O_3/Bi_2O_2CO_3$ photocatalyst for effective degradation of organic pollutions. Applied Catalysis B: Environmental. 2016;185:68–76.

[257] Ran R, McEvoy JG, Zhang Z. $Ag_2O/Ag_3VO_4/Ag_4V_2O_7$ heterogeneous photocatalyst prepared by a facile hydrothermal synthesis with enhanced photocatalytic performance under visible light irradiation. Materials Research Bulletin. 2016;74:140–150.

[258] Meng J, Yu Z, Li Y, Li Y. PdS-modified CdS/NiS composite as an efficient photocatalyst for H_2 evolution in visible light. Catalysis Today. 2014;225:136–141.

[259] Emeline A, Kuznetsov V, Ryabchuk V, Serpone N. On the way to the creation of next generation photoactive materials. Environmental Science and Pollution Research. 2012;19(9):3666–3675.

[260] Reszczyńska J, Grzyb T, Sobczak JW, Lisowski W, Gazda M, Ohtani B, et al. Visible light activity of rare earth metal doped (Er^{3+}, Yb^{3+} or Er^{3+}/Yb^{3+}) titania photocatalysts. Applied Catalysis B: Environmental. 2015;163:40–49.